Reactive absorption of CO2 in NaOH: Detailed study of enhancement factor models

Krauss, M.; Rzehak, R.;

Originally published:

March 2017

Chemical Engineering Science 166(2017), 193-209

DOI: https://doi.org/10.1016/j.ces.2017.03.029

Perma-Link to Publication Repository of HZDR:

https://www.hzdr.de/publications/Publ-24314

Reactive absorption of CO_2 in NaOH: Detailed study of enhancement factor models

Manuel Krauß, Roland Rzehak

Helmholtz-Zentrum Dresden – Rossendorf, Institute of Fluid Dynamics,
Bautzner Landstrasse 400, D-01328 Dresden, Germany

Abstract

In a pioneering study, Darmana et al. [Chemical Engineering Science 62 (2007), 2556 - 2575], considered the reactive absorption of CO_2 in aqueous NaOH in a bubble column. Although quite good agreement was obtained between an Euler-Lagrange simulation and measured pH-values at a single point, a number of aspects of the model deserve further discussion. This will be provided in the present work by using a simplified treatment that applies at the measurement location. Particularly relevant is the enhancement factor, which describes the effect of the chemical reaction on the mass transfer. An investigation of alternative expressions for this quantity is given, based on which an improved match with the data can be obtained. Furthermore, the complete network of possible reactions in this system has to be considered.

Keywords: mass transfer, chemical reaction, chemisorption, enhancement factor, dispersed gas liquid multiphase flow, modeling and simulation

1 INTRODUCTION

Due to its impact on global warming, the absorption of CO_2 from flue gas streams is nowadays an important consideration in energy production (Feron, 2016). It is also commonly used for gas purification applications in chemical engineering (Kohl and Nielsen, 1997). The industry standard is to use aqueous solutions of alkanolamines for this purpose (Rao and Rubin, 2002; Rochelle 2009). Reactions occurring in this system are quite complex involving formation of carbamate as well as carbonate and several related equilibria (e.g. Versteeg et al. 1996; Vaidya and Kenig, 2007; Couchaux et al. 2014). Therefore, process models based on integral balances have been developed (e.g. Kucka et al., 2003; Mandal et al., 2001; Pacheco and Rochelle, 1998), but no detailed simulations and experiments resolving local phenomena are available at present.

By using alkaline solutions the reactions are simplified, because carbamate formation is excluded and, aside from the auto-dissociation of water, only the carbonate-bicarbonate equilibrium needs to be considered. For the reactive absorption of CO_2 in aqueous NaOH or KOH in bubble columns, several detailed modeling and simulation studies by means of Euler-Euler or Euler-Lagrange methods have been published (Jain et al., 2015; Gruber et al., 2015; Zhang et al., 2009; Darmana et al., 2007; Bauer and Eigenberger, 2000; Marquez et al., 1999; Fleischer et al., 1996).

Concerning experimental investigations on such systems, Darmana et al. (2007) used own measurements of time-dependent pH-value at a single location in the column and an axial profile of mean bubble size to compare with their simulations. Becker (1996) provided measurements of time-dependent pH-value and temperature at four different heights in a bubble column. These data were used for comparison by Bauer and Eigenberger (2000) and Fleischer et al. (1996).

A rather detailed model for the reaction-kinetics and physico-chemical properties of the solution was presented by Darmana et al. (2007) together with expressions for the enhancement factor, mass transfer coefficient and effective diffusivity. Mostly the same models were used in the later works of Jain et al. (2015), Gruber et al. (2015) and Zhang et al. (2009). While the achieved level of agreement with the data was quite encouraging, the approximations implied by the modeling and their suitability for the problem at hand seem worth to be investigated in further detail.

In particular as will be shown, a frequently used approximation for the enhancement factor of an instantaneous irreversible second order reaction produces significant errors when used outside its range of applicability, which is restricted to situations with large enhancement effect. An improved fit formula with a rather wide range of application is presented. Moreover, it will be shown that the two-step nature of the reaction of CO_2 with hydroxide ions can be neglected for the conditions of Darmana et al. (2007), but examples for other conditions are given, where this is not justified. Finally, it will be shown that the reaction of CO_2 with water needs to be taken into account to correctly describe the later stage of the neutralization process.

For these purposes, a simplified description of the hydrodynamic phenomena in the bubble column is used which applies locally at the point of measurement. In this way possible errors of the present hydrodynamic modeling are excluded and the description of the chemistry can be assessed in isolation. A validation of this simplified approach is provided by comparison with the full Euler-Lagrange simulation results of Darmana et al. (2007).

A summary of the experimental and simulation results of Darmana et al. (2007) is given in section 2. The modeling of reactive mass transfer is described in section 3 detailing the complete network of possible reactions and different expressions for the enhancement factor available from the literature. Results of the calculations are presented in section 4.

Comparison is made with both experiments and simulations from Darmana et al. (2007). In addition, varied conditions are considered, namely the initial presence of dissolved sodium carbonate and an increased temperature. Conclusions and an outlook are given in section 5. Two appendices contain the correlations for reaction kinetics and physicochemical properties that were used and the development of the aforementioned fit formula for the enhancement factor of an instantaneous irreversible second order reaction.

2 SUMMARY OF RESULTS FROM DARMANA ET AL. (2007)

Darmana et al. (2007) investigated a lab scale bubble column of 200 mm width and 30 mm depth as sketched in Fig. 1. Initially the column was filled up to a level of 1000 mm with aqueous NaOH at a pH of 12.5. Pure CO_2 gas was supplied at a superficial velocity of 0.007 m/s through 21 needles arranged with a square pitch of 5 mm in the center of the column bottom. The size of the bubbles generated this way was d_B = 5.5 mm and an integral gas fraction of α_G = 1.2 % was obtained. The precise value of the temperature in the experiments was not reported.

The pH-value was measured by a glass electrode at a single point located 2 cm below the liquid surface in the center of the column. Bubble size was measured by videometry and bubble velocity by PIV over the entire column. Values of bubble size up to a height of approximately 40 cm of the column were judged as unreliable. In this region most bubbles appeared as clusters which could not be handled by the sizing algorithm, resulting in underestimated sizes. The integral gas hold-up was simply obtained from the difference of the liquid heights with and without aeration.

In addition to the experiment, Darmana et al. (2007) also presented simulation results using an Euler-Lagrange method. The calculated value for the integral gas fraction was α_G = 1.6 % which is somewhat too large compared with the experimental value of α_G = 1.2 %. For the cross-sectionally averaged bubble size at the top of the column, the simulations gave a value of d_B = 4.7 mm which is again somewhat too large compared with the experimental value of d_B = 3.5 mm.

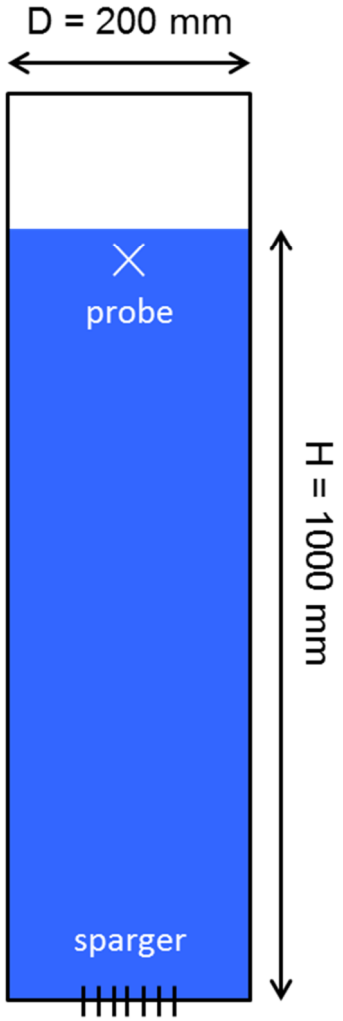

Figure 1: Sketch of geometry for the test from Darmana et al. (2007).

3 MODELING OF REACTIVE MASS TRANSFER

Mass transfer in a two-phase system is usually described by transport equations for the concentration of each solute species in both phases which are coupled by exchange terms. For the present purpose to quickly assess model alternatives and parameter sensitivities, a simplified model neglecting all spatial dependences is sufficient. In addition, only concentrations in the liquid phase need to be considered for this purpose. Thus in general terms, for each of the involved species, there is a single ordinary differential equation,

$$\frac{\partial}{\partial t}\left(\alpha_L \rho_L Y_L^X\right) = S_L^X + \Gamma_L^X . \tag{1}$$

Here, Y_L^X is the mass fraction of species X in the liquid phase at the measurement point, ρ_L is the density of the liquid mixture, and α_L is the liquid volume fraction. Assuming that the solvent is present in large excess, its mass fraction can be calculated from the constraint $\sum_X Y_L^X = 1$ and differential equations need to be solved only for the solute species. The source terms due to reaction, S_L^X, and due to transport across the phase interface, Γ_L^X, require further modeling as discussed below. For the source terms due to reaction, mass conservation requires that $\sum_X S_L^X = 0$. For absorption of species *X*, $\Gamma_L^X > 0$.

For bubbles consisting of pure CO_2 as in the experiment of Darmana et al. (2007) resistance to mass transfer occurs only on the liquid side. Then Γ_L^X is a function of the difference in concentration of the transferred species on the liquid side of the interface and in the bulk liquid. Using Henry' law to relate concentrations on the gas and liquid sides of the interface one gets

$$\Gamma_L^X = E\, k_L a_I \rho_L \left(He^X Y_G^X \frac{\rho_G}{\rho_L} - Y_L^X \right). \tag{2}$$

Models for the enhancement factor *E* are described in the next section. For the liquid side mass transfer coefficient k_L a correlation due to Brauer (1981)

$$k_L = \frac{D_L^X}{d_B}\left(2 + 0.015\ Re^{0.89} Sc^{0.7}\right), \tag{3}$$

is chosen over other possibilities (Rzehak, 2016) to match the simulations of Darmana et al. (2007). Here, Reynolds and Schmidt numbers are defined as $Re = u_{rel} d_B \rho_L \mu_L^{-1}$ and $Sc = \mu_L \left(\rho_L D_L^X\right)^{-1}$.

Assuming spherical bubbles the interfacial area concentration a_I can be obtained as

$$a_I = \frac{6\alpha_G}{d_B}. \tag{4}$$

The Henry constant He^X as well as the diffusion coefficient D_L^X are material properties for which correlations are taken from the literature as discussed in appendix A. Liquid density ρ_L and viscosity μ_L are taken as constants for the pure solvent assuming dilute solution. The gas density ρ_G is also taken as a constant corresponding to room conditions since pressure variations are small. Values for bubble size d_B, relative velocity u_{rel} = $|u_G$ - $u_L|$ and gas fraction α_G = 1-α_L are prescribed according to the experiment.

3.1 Reactions of CO2 in aqueous NaOH

Further discussion requires specification of the system to be considered, namely the reactive absorption of CO_2 in aqueous NaOH. The reactions of CO_2 in aqueous solution are rather well studied (e.g. Wang et al., 2010; Zeebe and Wolf-Gladrow, 2001; Stumm and Morgan, 1996). A diagram of the reaction network is shown in Fig. 2. It can be seen that there are two pathways, where the initial reaction is between the dissolved CO_2 and either hydroxide ions or water, respectively. Both result in a formation of bicarbonate ions which further react to form carbonate ions. It should be noted that the hydration reaction in the second branch can proceed either directly or via the formation of carbonic acid (Eigen et al., 1961). However, because it is neither possible nor necessary to distinguish between these two possibilities, it has been customary to simplify them to a single overall reaction (e.g. Sugai-Guérios et al., 2014; Johnson, 1982; Eigen et al., 1961) as shown on the diagram in Fig. 2. Here, the hydroxylation of CO_2 is denoted by a superscript I, the consecutive reaction which results in the formation of carbonate ions by a superscript II, and the hydration of CO_2 by a superscript III. Forward reactions are denoted by a superscript + and backward reactions by a superscript −.

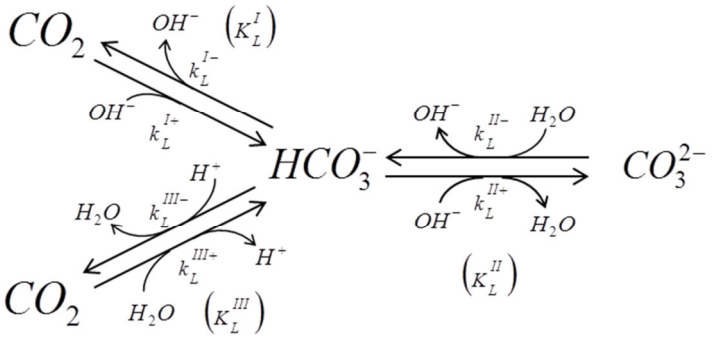

Figure 2: Reaction scheme of CO_2 in aqueous solution.

The relative importance of the two pathways, i.e. hydroxylation and hydration, depends on the pH-value. Only, the hydroxide path path was considered by Darmana et al. (2007), which dominates for pH > 10 (Kern, 1960).
It consists of two steps

$$CO_2 + OH^- \rightleftharpoons HCO_3^- , \quad (5)$$

which can be considered as irreversible, but proceeds at a finite rate, and

$$HCO_3^- + OH^- \rightleftharpoons CO_3^{2-} + H_2O , \quad (6)$$

which takes place instantaneously, but is reversible (Kern, 1960; Pinsent et al., 1956).
If the equilibrium of the second reaction Eq. (6) lies far on the right hand side, which may be expected in the initial stage of the chemisorption process due to the high pH values, this process may be described by a single irreversible overall reaction

$$CO_2 + 2\,OH^- \rightarrow CO_3^{2-} + H_2O . \quad (7)$$

The water path becomes important at pH < 10 and even dominant at pH < 8 (Kern, 1960). It also consists of two steps, the first of which, namely

$$CO_2 + H_2O \rightleftharpoons HCO_3^- + H^+ , \quad (8)$$

is reversible (Knoche, 1980; Kern, 1960)**.** The second step is the same as for the hydroxide path, i.e. Eq. (6).
Both pathways are coupled by the auto-dissociation of water

$$H_2O \rightleftharpoons OH^- + H^+, \tag{9}$$

which takes place instantaneously (Eigen, 1964).
Using the notation introduced in Fig. 2, the rates $R_L^{\Xi\pm}$ may be written as

$$R_L^{I+} = k_L^{I+} C_L^{CO_2} C_L^{OH^-} \tag{10}$$

$$R_L^{I-} = k_L^{I-} C_L^{HCO_3^-}. \tag{11}$$

$$R_L^{II+} = k_L^{II+} C_L^{HCO_3^-} C_L^{OH^-} \tag{12}$$

$$R_L^{II-} = k_L^{II-} C_L^{CO_3^{2-}}. \tag{13}$$

$$R_L^{III+} = k_L^{III+} C_L^{CO_2}. \tag{14}$$

$$R_L^{III-} = k_L^{III-} C_L^{HCO_3^-} C_L^{H^+} = k_L^{III-} C_L^{HCO_3^-} \frac{K_W}{C_L^{OH^-}}. \tag{15}$$

Note that $R_L^{\Xi\pm}$ is always in units of [kmol m^{-3} s^{-1}], but units of the rate constant $k_L^{\Xi\pm}$ depend on the reaction order. In Eqs. (13) and (14) it is assumed that the solvent, H_2O, is present in large excess so that its concentration does not change appreciably during the reaction. Due to the ionization of water with its equilibrium constant K_W the molar concentration of hydrogen ions in Eq. (15) can be replaced by the concentration of hydroxide ions as shown above. A model for the rate and equilibrium constants in this reaction system is detailed in appendix A**.**

X	S_L^X	Γ_L^X
CO_2	$M^{CO_2}(-R^{I+}+R^{I-}-R^{III+}+R^{III-})$	$\neq 0$
$(Na^+)OH^-$	$M^{OH^-}(-R^{I+}+R^{I-}-R^{II+}+R^{II-}-R^{III+}+R^{III-})$	0
$(Na^+)HCO_3^-$	$M^{HCO_3^-}(+R^{I+}-R^{I-}-R^{II+}+R^{II-}+R^{III+}-R^{III-})$	0
$(2Na^+)CO_3^{2-}$	$M^{CO_3^{2-}}(+R^{II+}-R^{II-})$	0

Table 1: Summary of species and source terms for the absorption of CO_2 in aqueous NaOH.

The chemical species involved in the process are listed in Table 1. Na^+ does not participate in the reactions, but its presence has to be considered in reaction rates and material properties. The source terms due to reaction, S_L^X in Eq. (1), are given in Table 1 in terms of the reaction rates Eqs. (10) – (15). The source term due to transport across the phase interface, Γ_L^X in Eq. (1), appears only for the unreacted CO_2. Effects of the chemical reaction on the mass transfer are included in this term by means of an enhancement factor, which may be obtained from either film, penetration, or renewal models as described below. Once the CO_2 is dissolved in the water no further distinction is made between film and bulk liquid such that a seamless treatment of fast and slow reaction regimes is possible.

3.2 Enhancement factor models

The enhancement factor is defined as the ratio between mass fluxes through the phase interface with and without reaction, based on the same driving force of concentration (e.g. Westerterp et al., 1987). Obviously it depends on the reaction considered, in particular whether it is single- or multi-step, reversible or irreversible, slow or fast or even instantaneous, and finally first or second or higher order. Models for enhancement factors have so far been derived predominantly from simple conceptual models of mass transfer, namely the film, penetration, and renewal models (e.g. Danckwerts, 1970). To obtain practically applicable results, significant approximations have to be introduced for almost all cases. Results relevant to the present reaction system are discussed in the following.

First, a fast single-step irreversible reaction of second order $A + \nu_B B \rightarrow Q$ is considered. This corresponds to the overall reaction Eq. (7), where A corresponds with CO_2, B with OH^-, and Q with CO_3^{2-}. The stoichiometric factor of OH^- in this reaction is $\nu_B = 2$, but the reaction is still of first order in both reactants. The Hatta number thus is

$$Ha = \frac{\sqrt{k_L^{I+} D_L^A C_L^B}}{k_L}. \tag{16}$$

Because of the irreversibility, the products Q do not matter.

Based on the renewal model, an expression for the enhancement factor for this case has been derived by DeCoursey (1974) as

$$E = -\frac{Ha^2}{2(E_i - 1)} + \sqrt{\frac{Ha^4}{4(E_i - 1)^2} + E_i \frac{Ha^2}{(E_i - 1)} + 1}\,. \tag{17}$$

Unless the condition $E_i \geq 1$ is violated, Eq. (17) will always give values for E which are greater or equal to one. Otherwise values are limited by using $\max(E,1)$ (Westerterp et al., 1987). An expression based on the penetration model has been found by Hikita and Asai (1964) as

$$E = \left(Ha\ \eta + \frac{\pi}{8 Ha\ \eta} \right)\ erf\left(\frac{2 Ha\ \eta}{\sqrt{\pi}} \right) + \frac{1}{2} exp\left(-\frac{4 Ha^2 \eta^2}{\pi} \right), \tag{18}$$

and based on the film model, Van Krevelen and Hoftijzer (1948) and Brian et al. (1961) found

$$E = \frac{Ha\ \eta}{\tanh(Ha\ \eta)}, \tag{19}$$

where $\eta = \sqrt{(E_i - E)/(E_i - 1)}$.

All of these expressions involve the enhancement factor for an instantaneous reaction E_i of the type of Eq. (7). The first expression, Eq. (17), is explicit, while the two others, Eqs. (18) and (19), are implicit, i.e. require the solution of a non-linear algebraic equation, which can be done conveniently e.g. in MatLab.

A comparison of all three expressions is shown in Fig. 3, where the explicit expression of Eq. (17) has been used as a reference. For the purpose of this comparison, E_i was treated simply as a parameter. It can be seen that over a wide range of values for Ha and E_i, the differences

between all three expressions are only minor. Thus, regardless of which model – film, penetration, or renewal – is used, Eq. (17) at least provides a convenient fit formula.

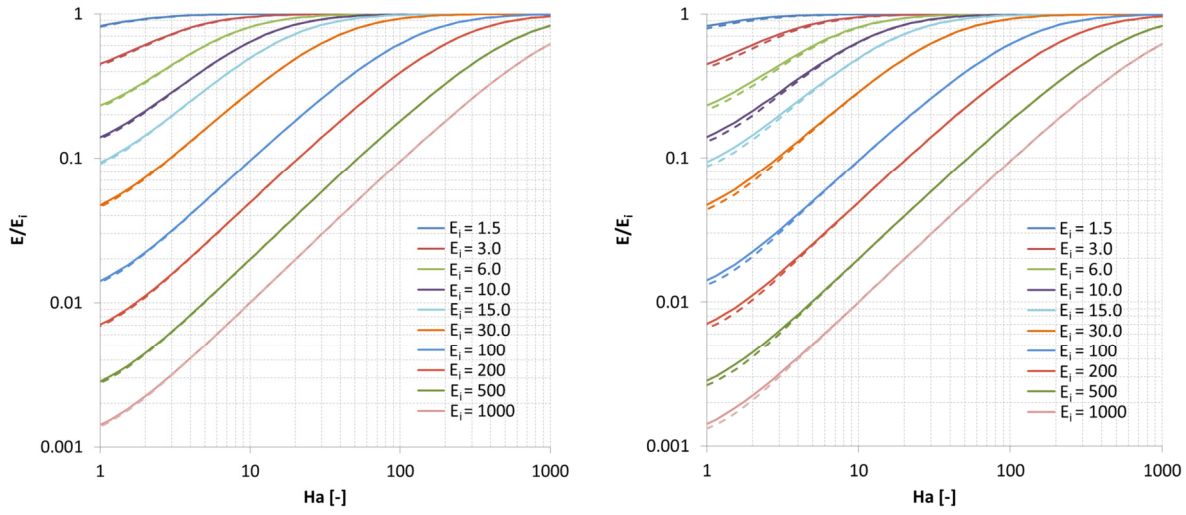

Figure 3: Comparison of enhancement factors for a fast irreversible second order reaction obtained by different models for different values of *Ha* and E_i. a) penetration model Eq. (18) (dashed lines) versus renewal model Eq. (17) (solid lines); b) film model Eq. (19) (dashed lines) versus renewal model Eq. (17) (solid lines).

To apply any of the models for the enhancement factor discussed above, an expression for the case of an instantaneous reaction, E_i, is needed. A solution that applies to both the penetration and renewal models has been given by Danckwerts (1970) as

$$E_i = \frac{1}{\operatorname{erf}\left(\beta / \sqrt{D_L^A}\right)} = \frac{\operatorname{erf}\left(\beta / \sqrt{D_L^B}\right)}{\operatorname{erf}\left(\beta / \sqrt{D_L^A}\right)} + \frac{\exp\left(-\beta^2 / D_L^B\right)}{\exp\left(-\beta^2 / D_L^A\right)} \frac{C_{L,\infty}^B}{\nu^B C_{L,I}^A} \sqrt{\frac{D_L^B}{D_L^A}} . \tag{20}$$

In general the second equation needs to be solved for β first, before evaluating the first equation for E_i. Results are shown as the solid lines in Fig. 4.
An analytical solution is possible for $D^A = D^B$, where β drops out in Eq. (20) and E_i becomes

$$E_i = 1 + \frac{C_{L,\infty}^B}{\nu^B C_{L,I}^A} . \tag{21}$$

For the case $\beta \to 0$ corresponding to $E_i \to \infty$, a direct evaluation of Eq. (20) is also possible by calculating the limit of the first term on the right hand side according to de l'Hospitals rule (e.g. Jeffrey, 2005). This gives an approximate explicit expression valid for $E_i >> 1$ as

$$E_i = \sqrt{\frac{D_L^A}{D_L^B}} + \frac{C_{L,\infty}^B}{\nu^B C_{L,I}^A} \sqrt{\frac{D_L^B}{D_L^A}} = \left(1 + \frac{D_L^B C_{L,\infty}^B}{\nu^B D_L^A C_{L,I}^A}\right) \sqrt{\frac{D_L^A}{D_L^B}} . \tag{22}$$

This expression is shown as the dashed lines in Fig. 4a). For $D^A = D^B$ Eq. (22) agrees with the exact result Eq. (21), but otherwise reasonable accuracy requires $E_i \geq 2 \ldots 10$ depending on the value of D^A / D^B. In general Eq. (22) is not even guaranteed to satisfy the requirement $E_i \geq 1$. Therefore, the first term is sometimes changed to 1, i.e.

$$E_i = 1 + \frac{C^B_{L,\infty}}{\nu^B C^A_{L,I}} \sqrt{\frac{D^B_L}{D^A_L}}, \tag{23}$$

which gives the fat solid line in Fig. 4 irrespective of the true value of D^A / D^B. Depending on this value the error may still be significant, but at least it remains bounded as E_i approaches 1. The approximations Eqs. (22) and (23) are frequently quoted in reaction engineering textbooks (e.g. Westerterp et al., 1987), but their error should be carefully checked for each application.

An explicit fit-formula that reproduces the numerical solution of the implicit Eq. (20) with engineering accuracy over a large range of parameters is developed in appendix B. A comparison between both is shown as the dashed lines in Fig. 4b).

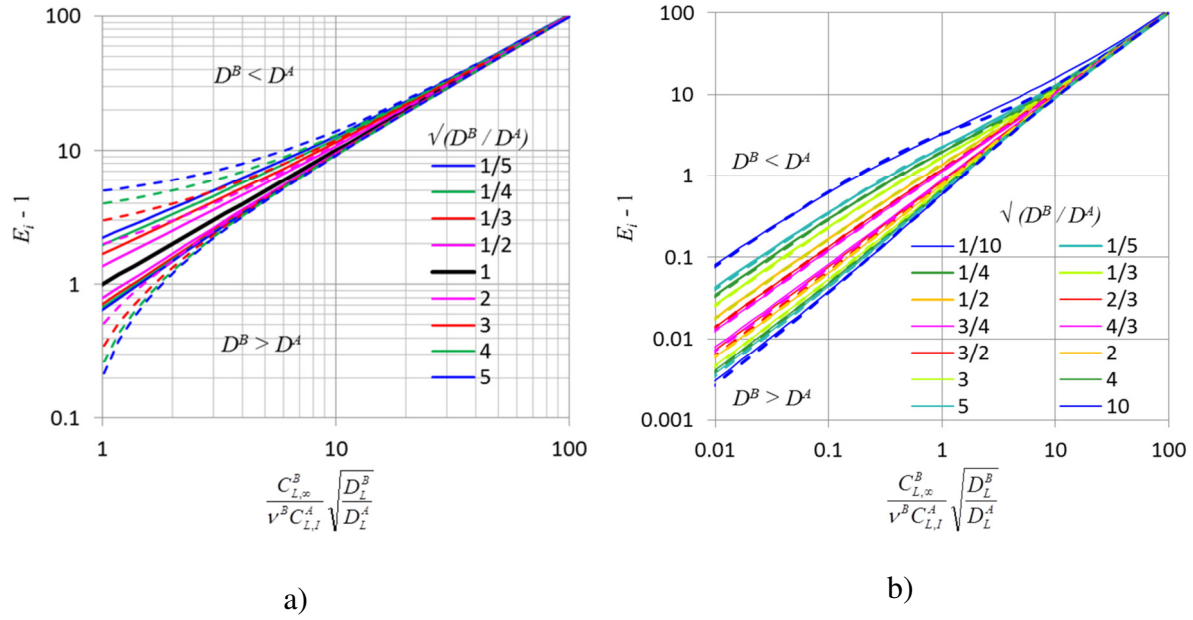

Figure 4: Comparison of expressions for the enhancement factor of an instantaneous second order reaction. a) Solid lines: numerical solution of the implicit equation Eq. (20); dashed lines: explicit approximation Eq. (22). b) Solid lines: numerical solution of the implicit equation Eq. (20); dashed lines: explicit fit formula Eqs. (B.4)-(B.6).

For the film model Sherwood and Pigford (quoted by Brian et al., 1961) and Hikita and Asai (1964) found

$$E_i = 1 + \frac{D^B_L C^B_{L,\infty}}{\nu^B D^A_L C^A_{L,I}}. \tag{24}$$

For $D^A = D^B$ this agrees with the exact result for the penetration model Eq. (21), but otherwise the dependence on the diffusion coefficients is wrong, which is typical for expressions obtained by using the film model (e.g. Cussler, 2007, Bird et al, 2002). An ad hoc change to a square root dependence on D^A and D^B is frequently found to give good results

(Glasscock and Rochelle, 1989; Chang and Rochelle, 1982; Brian et al., 1961; Olander, 1960). If this heuristic is applied to Eq. (24), one recovers Eq. (23). As discussed above, depending on the value of D^A / D^B this expression may not be very accurate. However to avoid at least the worst inaccuracies, this replacement should nonetheless always be done with film model results.

The full two-step reaction Eqs. (5) – (6), is of the form A + B $\rightarrow$ P, P + B $\leftrightarrow$ Q, where in addition to the above, P corresponds with HCO_3^-. For such a system, results based on both the film and penetration models have been obtained by Hikita and Asai (1976a) while no treatment based on the renewal model is known.

For the penetration model,

$$E = \left(Ha\ \eta + \frac{\pi}{8Ha\ \eta} \right)\ erf\left(\frac{2Ha\ \eta}{\sqrt{\pi}} \right) + \frac{1}{2}\exp\left(-\frac{4Ha^2\eta^2}{\pi} \right), \tag{25}$$

while for the film model,

$$E = \frac{Ha\ \eta}{\tanh\left(Ha\ \eta\right)}, \tag{26}$$

where

$$\eta = \left(\sqrt{\frac{1}{4}\left(\frac{E - E_i}{E_i - 1} + \sqrt{\frac{D_L^P}{D_L^B}}\ \frac{C_{L,\infty}^P}{C_{L,\infty}^B} + \sqrt{\frac{D_L^P}{D_L^Q}}\ \frac{C_{L,\infty}^P}{C_{L,\infty}^Q} \right)^2 - \left(\frac{E - E_i'}{E_i' - 1} \right)\left(\sqrt{\frac{D_L^P}{D_L^B}}\ \frac{C_{L,\infty}^P}{C_{L,\infty}^B} + \sqrt{\frac{D_L^P}{D_L^Q}}\ \frac{C_{L,\infty}^P}{C_{L,\infty}^Q} \right)} \right.$$

$$\left. - \frac{1}{2}\left(\frac{E - E_i}{E_i - 1} + \sqrt{\frac{D_L^P}{D_L^B}}\ \frac{C_{L,\infty}^P}{C_{L,\infty}^B} + \sqrt{\frac{D_L^P}{D_L^Q}}\ \frac{C_{L,\infty}^P}{C_{L,\infty}^Q} \right) \right)^{\frac{1}{2}} \tag{27}$$

Note that Eqs. (25) and (26) are exactly the same as Eqs. (18) and (19) for the single-step reaction, only the definition of η is changed.

Both expressions involve the enhancement factors E_i for an instantaneous reaction where both steps are irreversible and E_i' for an instantaneous reaction where the first step is irreversible but the second is reversible. Expressions for E_i and E_i' will be given shortly. Also both expressions Eqs. (25) and (26) are implicit.

A comparison of Eqs. (25) and (26) as functions of $Ha \cdot \eta$ is shown in Fig. 5. It can be seen that the differences are only minor.

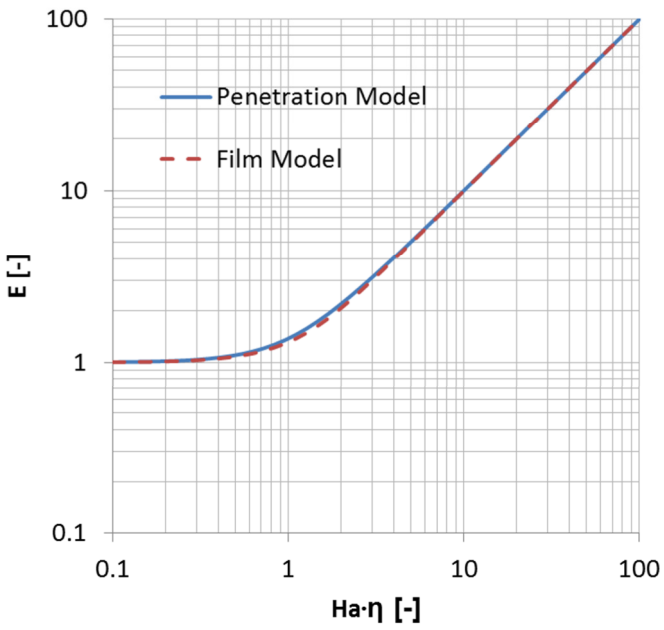

Figure 5: Comparison of expressions for the enhancement factor of the two-step reaction Eqs. (5) – (6). Solid line: penetration model according to Eq. (25); dashed line: film model according to Eq. (26).

For the penetration model E_i is given by the same expression as for the one-step reaction, namely Eq. (20). E_i' is determined from

$$E_i' = \frac{1}{\operatorname{erf}\left(\beta_1' / \sqrt{D_L^A}\right)} \tag{28}$$

$$= \frac{\operatorname{erf}\left(\beta_2' / \sqrt{D_L^B}\right)}{\operatorname{erf}\left(\beta_1' / \sqrt{D_L^A}\right)} + \frac{C_{L,\infty}^B}{\nu^B C_{L,I}^A} \sqrt{\frac{D_L^B}{D_L^A}} \frac{\exp\left(\beta_1'^2 / D_L^A + \beta_2'^2 / D_L^P\right)}{\exp\left(\beta_1'^2 / D_L^P + \beta_2'^2 / D_L^B\right)}$$

$$= \frac{\operatorname{erf}\left(\beta_1' / \sqrt{D_L^Q}\right)}{\operatorname{erf}\left(\beta_1' / \sqrt{D_L^A}\right)} + \frac{C_{L,\infty}^Q}{C_{L,I}^A} \sqrt{\frac{D_L^Q}{D_L^A}} \frac{\exp\left(\beta_1'^2 / D_L^A\right)}{\exp\left(\beta_1'^2 / D_L^Q\right)} + 2 \frac{1 - \operatorname{erf}\left(\beta_2' / \sqrt{D_L^Q}\right)}{\operatorname{erf}\left(\beta_1' / \sqrt{D_L^A}\right)} \frac{\exp\left(\beta_1'^2 / D_L^P + \beta_2'^2 / D_L^Q\right)}{\exp\left(\beta_1'^2 / D_L^Q + \beta_2'^2 / D_L^P\right)}$$

Here, the second and third equations have to be solved for β_1' and β_2' first, before evaluating the first equation for E_i'.
For the film model E_i is again given by the same expression as for the one-step reaction, namely Eq. (24). E_i' is determined from

$$E_i' = 1 + \frac{C_{L,\infty}^B}{C_{L,I}^A} \frac{D_L^B}{D_L^A} + \frac{C_{L,\infty}^Q}{C_{L,I}^A} \frac{D_L^Q}{D_L^A}. \tag{29}$$

As suggested before, the film model should always be used with the heuristic replacement of the dependence on the diffusivities by square roots rather than linear dependence to avoid at least the worst inaccuracies.

4 RESULTS AND DISCUSSION

The simplified model described in section 3, i.e. the system of equations Eq. (1) for the species and reactions summarized in Table 1 together with Eqs. (2) – (4) for the mass transfer is solved using MatLab again.

The parameter values used with this model are as follows. The initial OH^- and Na^+ mass concentrations are taken to be equal and determined by the initial pH-value of 12.5. All other mass concentrations of the species dissolved in the liquid phase are set to a tiny positive value to avoid divisions by zero. Since the temperature was not expressly given in Darmana et al. (2007), it is set to a constant value of 25°C. The density and molecular viscosity of pure water at that temperature are 997 kg m^{-3} and 0.890 mPa s. The mixture is assumed to be dilute so that these values also apply for the mixture. The gas phase is supposed to behave as an ideal gas.

It is assumed that the integral gas hold up of α_G = 1.2 % reported by Darmana et al. (2007) represents the gas volume fraction at the measurement point. Moreover the bubble diameter at this position is estimated as d_B = 3.5 mm using the bubble size distribution shown in figure 13 of Darmana et al. (2007). According to the well-known diagram of Clift et al. (1978), a relative velocity of about u_{rel} = 0.23 m/s is expected. Finally, the bubble diameter and gas volume fraction at the measurement point are taken as constant, although both are expected to increase in time, because the absorption process slows down as saturation is approached.

model	expression for E	expression for E_i
1A	one-step, renewal model, Eq. (17)	approximate formula Eq. (22)
1B	one-step, renewal model, Eq. (17)	implicit Eq. (20)
1C	one-step, renewal model, Eq. (17)	explicit fit formula Eqs. (B.4)-(B.6)
2A	two-step, penetration model, Eqs. (25) and (27)	implicit Eqs. (20) and (28)
2B	two-step, film model, Eqs. (26) and (27)	explicit Eqs. (24) and (29) with square root dependence on D^A / D^B

Table 2: Investigated enhancement factor models.

Based on the discussion of section 3.3, a number of different models for the enhancement factor are considered. An overview is given in Table 2. Model 1A uses the expression for the enhancement factor for the one-step overall reaction Eq. (7) based on the renewal model, Eq. (17), together with the approximate formula Eq. (22) for the instantaneous limit. This is the same enhancement factor model as used by Darmana et al. (2007). As shown in section 3, the accuracy of the approximation Eq. (22) is only acceptable if E_i is sufficiently large. Otherwise, numerical evaluation of the implicit equation Eq. (20) or the fit formula from Appendix B should be used. This is done in models 1B and 1C, respectively. Models 2A and 2B, finally, use the available expressions for the enhancement factor accounting for the two-step nature of the reactions Eqs. (5) and (6). For the penetration model, 2A, expression Eq. (25) together with (27) is complemented by numerical evaluation of the implicit equations Eqs. (20) and (28) for the instantaneous limits. For the film model, 2B, expression Eq. (26) together with (27) is complemented by the explicit equations Eqs. (24) and (29) where dependences on D^A and D^B have been changed to square roots. It should be noted that all of these models consider only the reaction of CO_2 with hydroxide ions (see section 3.2).

Effects of including the water pathway as well will be investigated separately, since this reaction is too slow to cause an enhancement of the mass transfer.

4.1 Validation of simplified approach

As a first step in the investigation, we demonstrate that the simplified pointwise approach gives reasonable results by comparing it with the results of the full Euler-Lagrange simulations of Darmana et al. (2007). For this comparison the same enhancement factor model as in Darmana et al. (2007) is applied, i.e. model 1A in Table 2. Moreover, in addition to the experimental values given above, the average gas volume fraction and bubble diameter of $\alpha_G = 1.6$ % and $d_B = 4.7$ mm obtained in the simulations of Darmana et al. (2007) are used as well. As shown in Fig. 6, the simplified model using these parameter values (smooth solid lines) gives results that exactly match the simulations of Darmana et al. (2007) (thick dots) for the pH and are very close to them for the other species concentrations. Therefore, despite the simplifications made, the pointwise model is suitable to assess different alternatives in modeling mass transfer and chemical reaction.
Changing gas volume fraction and bubble diameter to the experimentally determined values has only a small effect. The difference between the pH-values calculated by the simplified model using these parameters (dashed lines) and the ones measured by Darmana et al. (2007) (noisy solid line) remains almost unchanged. To further investigate how this gap can be closed, the experimentally determined gas volume fraction and bubble diameter will be used in the following.

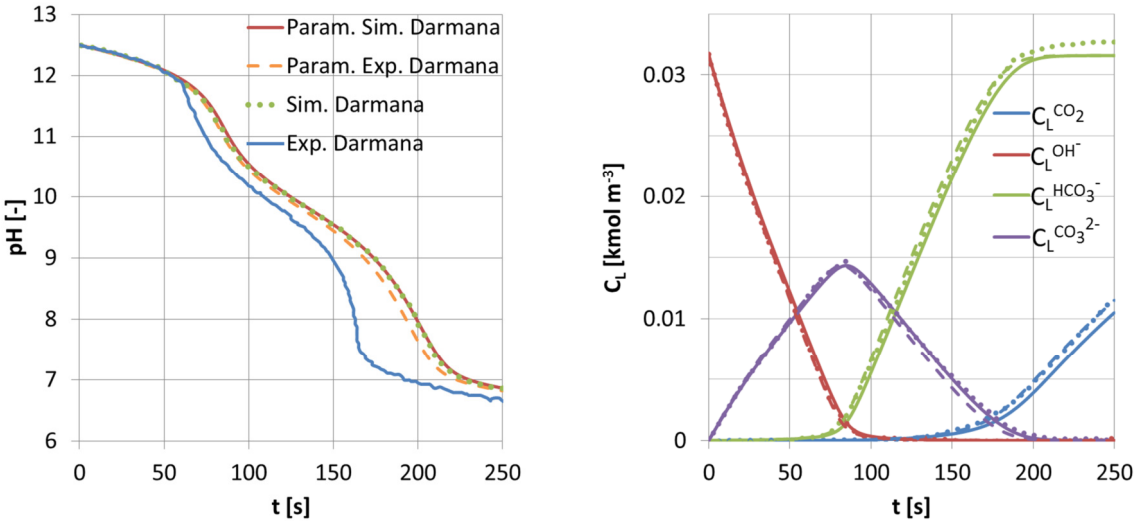

a) b)

Figure 6: Results of the simplified pointwise model using simulated $\alpha_G = 1.6$ % and $d_B = 4.7$ mm (smooth lines) and experimentally determined $\alpha_G = 1.2$ % and $d_B = 3.5$ mm (dashed lines) given by Darmana et al. (2007), compared with Euler-Lagrange simulations (thick dots) and measured values (noisy solid line) of Darmana et al. (2007). For the enhancement factor, model 1A in Table 2 is used, matching the work of Darmana et al. (2007). a) Time-dependent pH-value; b) time-dependent species concentrations.

4.2 Comparison of Enhancement Factor Models

Next, we present a comparison of the five different enhancement factor models summarized in Table 2. In Fig. 7, the thick dots and noisy solid line again represent the simulations and experiments of Darmana et al. (2007) while the smooth solid line gives the present results for model 1A. Compared to model 1A it can be seen the results for all other models come closer to the experimentally determined pH-values. These other models now give good agreement with the experiment up about 150 s although the kink in the measured data at ~60 s is missed. Differences between the models except 1A are only minor.
The improvement of models 1B and 1C over model 1A clearly demonstrates the inadequacy of the approximation Eq. (22) for the instantaneous enhancement factor. Curves for models 1B and 1C completely overlap each other for the entire range of times considered. This proves the suitability of applying the explicit fit formula obtained in Appendix B instead of a numerical evaluation of the implicit equation Eq. (20). Hence from the two, only model 1C will be considered further.
The agreement of the results for models 2A and 2B with model 1C means that for the conditions considered, the two-step nature of the reaction does not play a significant role. Differences between penetration and film model for the two-step reaction are only minor, with the latter (2B) giving marginally smaller values than the former (2A).

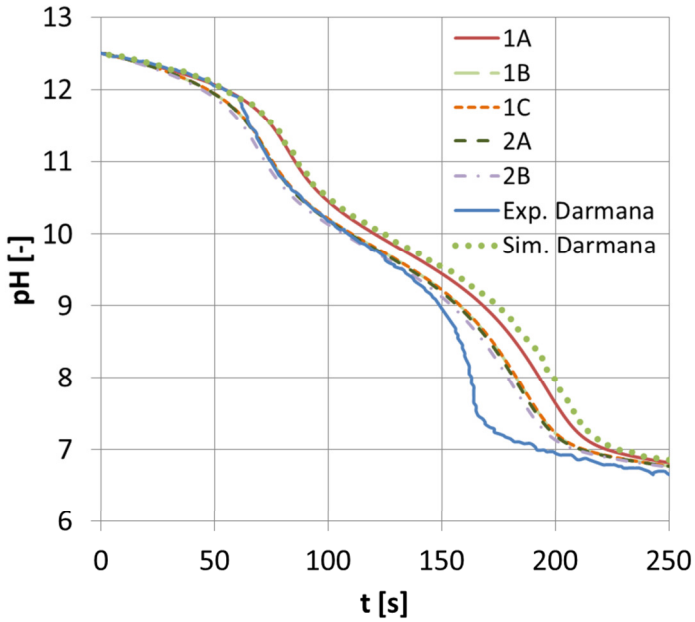

Figure 7: Comparison of results for time-dependent pH-value obtained from the simplified pointwise calculation using different enhancement factor models (see Table 2 for description). Euler-Lagrange simulations (thick dots) and measured values (noisy solid line) of Darmana et al. (2007) are shown again for comparison.

Understanding the reasons for the observed effects using different enhancement factor models is possible by comparing the resulting values of the time-dependent enhancement factors, Hatta numbers, species concentrations, gas absorption rates and effective reaction rates. Effective reaction rates are characterized by the difference of the forward and backward reaction rate, whereby a positive sign means domination of the forward reaction, while for a

negative sign the backward reaction predominates. Because the results for models 1B and 1C are identical, model 1B is not further considered in this discussion. Consistent with the similarity of the time-dependent pH-values for models 1C, 2A and 2B, the time-dependent species concentrations and reaction rates are also very similar. Thus it suffices to compare the concentrations and reaction rates for models 1A and 1C. The results are shown in Fig. 8.

Looking first at the Hatta numbers shown in Fig. 8 a) and b), it is seen that for all models the values decrease over time. Up to a time of ~80 s this decrease is rather steep, while afterwards it becomes more gradual. This is due to the decrease in the concentration of hydroxide ions as they are consumed during the reaction, which appears in the definition of *Ha* (see Eq. (16)). Values are very similar for models 1C, 2A, and 2B, while for model 1A somewhat higher values are found. This is due to the somewhat higher concentration of hydroxide ions (see Fig. 8c)) for model 1A resulting from the smaller enhancement factor obtained for that model as will be discussed in the following.

Comparing the time-dependent enhancement factors for models 1A and 1C in Fig. 8 a), it is evident that the enhancement factors decrease with decreasing Hatta numbers as expected, but the enhancement factors for model 1C are notably higher than for model 1A. In particular, the small values of E_i for model 1A, which even become less than one, clearly demonstrate that the approximation for E_i is not suitable here. Also the temporal evolution of E is different for models 1A and 1C. For model 1A the decrease in enhancement is approximately linear and its minimum value of one is reached rather abruptly after about 40 s without relation to the evolution of Ha. For model 1C the enhancement shows a less steep decrease and is effective until a time of ~80 s where the decrease of the Hatta number levels of as well at a value of $Ha \approx 0.3$.

The time-dependent enhancement factors for models 2A and 2B are shown in Fig. 8 b). While the time-dependent Hatta numbers are almost exactly the same for both of these models, the enhancement factors differ slightly from each other, with the film model, 2B, resulting in higher values than the penetration model, 2A. As has been shown in Fig. 5, the values of E as a function of $Ha \cdot \eta$ are also almost exactly the same. Therefore, the differences must be due to the different expressions for E_i and E_i'.

Comparing the enhancement factor for models 2A and 1C between Figs. 8b) and 8a), almost the same values are found. The one-step enhancement factor model is applicable if all intermediate bicarbonate ions are further transformed into the final product, the carbonate ions. As will be discussed shortly, this requirement is effectively fulfilled from t = 0 s to about 70 s. Coincidentally, significant enhancement also occurs only within this time range.

Turning now to the effective reaction rates shown in Fig. 8 d), the following qualitative behaviour is seen. As long as an enhancement of the mass transfer takes place, i.e. up to a time of ~40 s for model 1A and ~70 s for model 1C, the curves for the effective rate of reaction I overlap with those of the gas absorption rate. This means, all absorbed CO_2 molecules react with hydroxide ions to form bicarbonate ions. These in turn react with other hydroxide ions to form carbonate ions as long as the effective rate of reaction II remains positive and the transformation is almost complete if the effective rate of reaction II is of the same order of magnitude as that of reaction I. Due to the steep drop of the effective rate of reaction II in Fig. 8d) both conditions hold to a good approximation until a time of ~80 s for model 1A and ~70 s for model 1C. From the start of the absorption process up to this time, the overall reaction Eq. (7) occurs.

In the species concentrations of Fig. 8c) this shows up by a consumption of hydroxide ions which is about twice as high as the production of carbonate ions and negligible presence of bicarbonate ions or aqueous CO_2 up to times of ~80 s and ~70 s for models 1A and 1C, respectively. At these times a peak in the concentration of carbonate ions is reached corresponding to the reversal of the sign of the effective rate of reaction II. After this point,

the backward reaction II becomes dominant and the formation of bicarbonate ions sets in. The effective rates of reactions I and II then are almost equal and opposite, but reaction I is still consuming more hydroxide ions than released by reaction II as evidenced by the still decreasing pH-value. As long as the solution contains a significant amount of hydroxide ions, reaction I proceeds and most of the absorbed CO_2 is reacted away. This leads to an almost constant concentration gradient at the phase interface and consequently a constant absorption rate. When reaction I becomes weaker and finally almost stops, reaction II follows the same trend due to its instantaneous equilibration, so that the CO_2 concentration starts to increase with the same rate at which it is absorbed from the gas phase.

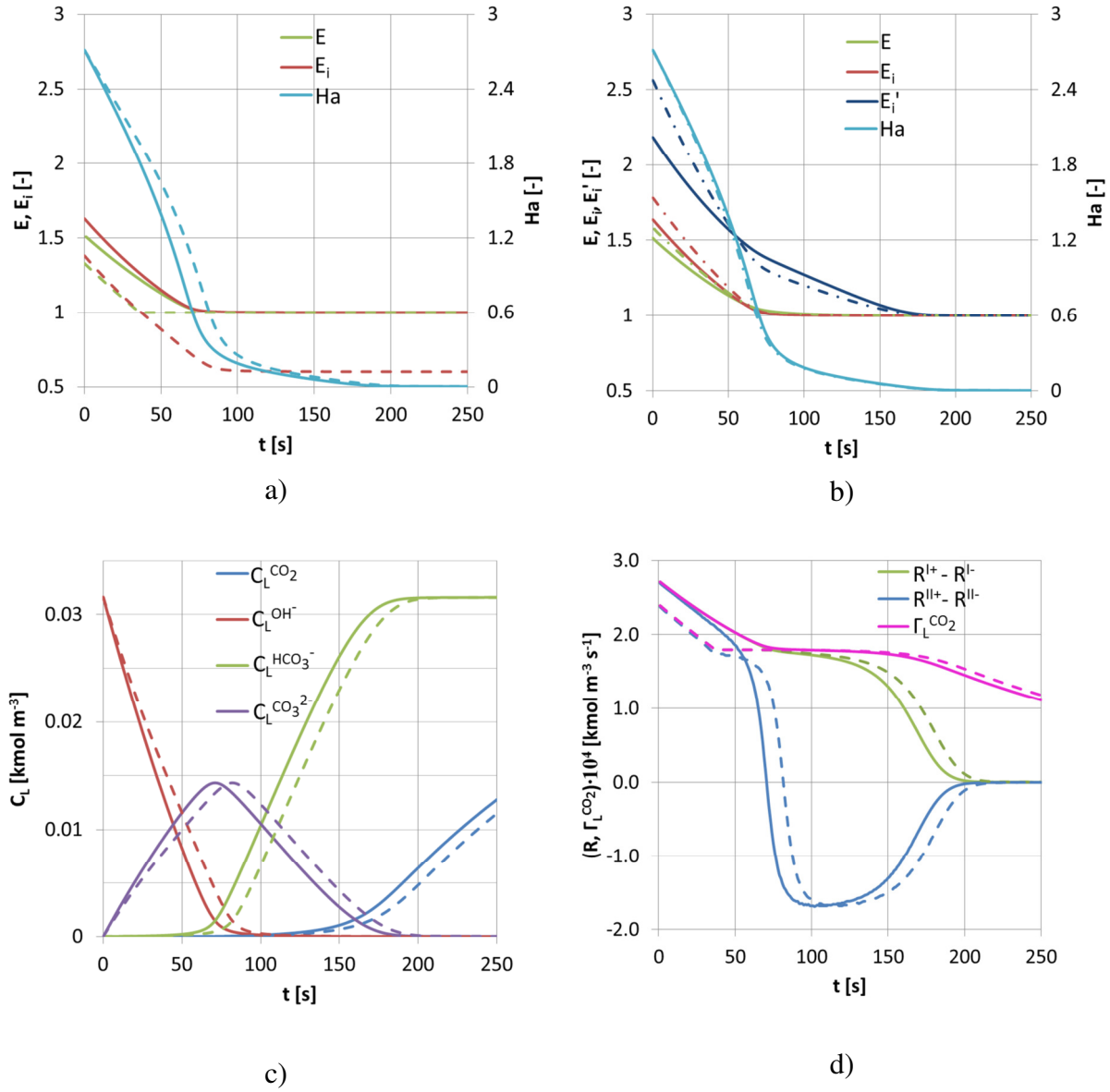

Figure 8: Comparison of results obtained from the simplified pointwise calculation: a) time-dependent enhancement factors and Hatta number for model 1A (dashed lines) and model 1C (solid lines). b) time-dependent enhancement factors and Hatta number for model 2A (solid lines) and model 2B (dash-dotted lines) c) time-dependent species concentrations for model 1A (dashed lines) and model 1C (solid lines), d) time-dependent reaction and absorption rates for model 1A (dashed lines) and model 1C (solid lines).

4.3 Effect of initially added sodium carbonate

The surprisingly small difference in the results of Fig. 7 for the enhancement factor models based on one- and the two-step reactions motivates a further investigation of conditions where effects of reaction II become significant. Two ways to realize such conditions come to mind. First, by decreasing the value of the equilibrium constant K^{II}, which can be achieved experimentally by increasing the temperature. Second, by adding sodium carbonate to the initial solution, which has a similar effect to increase the backward rate of reaction II. The first possibility will be discussed in section 4.4. The consequences of the second possibility are demonstrated in Fig. 9.

A rather high value for the initial sodium carbonate concentration of 1 kmol m^{-3} was found necessary to produce a sizeable effect. It should be noted that an increased concentration of ions also causes a strong increase of the forward rate of reaction I by a factor of about 3, a reduction of the CO_2 solubility by ~50% and a decrease of the CO_2 diffusivity of ~25% (see Appendix A). All of these effects act together with the increased carbonate concentration.

Fig. 9a) shows a comparison of the species concentrations for the cases with (dashed lines) and without (solid lines) initial carbonate ions calculated using the enhancement factor model 2A which is appropriate for the two-step reaction. For the carbonate ions, the difference to the initial concentration is shown to improve comparability. It is seen that initially along with the added carbonate ions, there are also some more hydroxide and bicarbonate ions present. This is due to the instantaneous equilibration of reaction II.

The carbonate concentration at first increases and goes through a maximum at times of ~110 s with and ~70 s without added carbonate. At the peak of the carbonate concentration, the bicarbonate concentration profile reaches its highest slope. The later stage of the process, where the bicarbonate concentration reaches its final value and the concentration of dissolved CO_2 begins to rise, is beyond the monitoring period for the case with added carbonate. The slower progression of the absorption process with added carbonate is caused by the fact that mass transfer is the limiting step and the solubility decreases upon addition of the carbonate.

The increase in the carbonate concentration corresponds with a positive value of the effective rate of reaction II as shown in Fig. 9b). However, comparing the cases with and without added carbonate, the effective rate of reaction II is clearly reduced upon the addition of the carbonate and shows a more gradual temporal progress. Furthermore, in the initial stage, the difference between the effective rates of reactions I and II is increased. This corresponds with a higher concentration of bicarbonate and hydroxide visible in Fig. 9a). At the time where the carbonate concentration reaches its maximum, the effective rate of reaction II changes its sign for both cases. Again, the later stage of the process, where both reactions come to a halt, i.e. their effective rates vanish, is beyond the monitoring period for the case with added carbonate.

With added carbonate, the reduced consumption of hydroxide ions by reaction II together with the increased rate constant of reaction I, k_L^{I+}, due to the higher ionic strength results in larger enhancement factors and a larger value of the Hatta number as shown in Fig. 9c). After ~50 s, E even becomes greater than E_i. Clearly this is only possible due to the presence of E_i' in the two-step enhancement factor model 2A, which assumes a large value of $E_i' \approx 50$ that changes only little throughout the monitoring period (not shown in the figure for the sake of clarity).

In Fig. 9d) finally, a comparison of enhancement factors and Hatta number is given between the two-step model 2A and the simpler one-step model 1C. It is seen that the initial values of Hatta number and E_i are almost the same, but the enhancement factor E is notably higher for the two-step model 2A and this difference becomes greater with temporal progress. Again

this must be due to the presence of E_i' in the two-step model 2A. This shows that a one-step model is not suitable for the case with added carbonate.

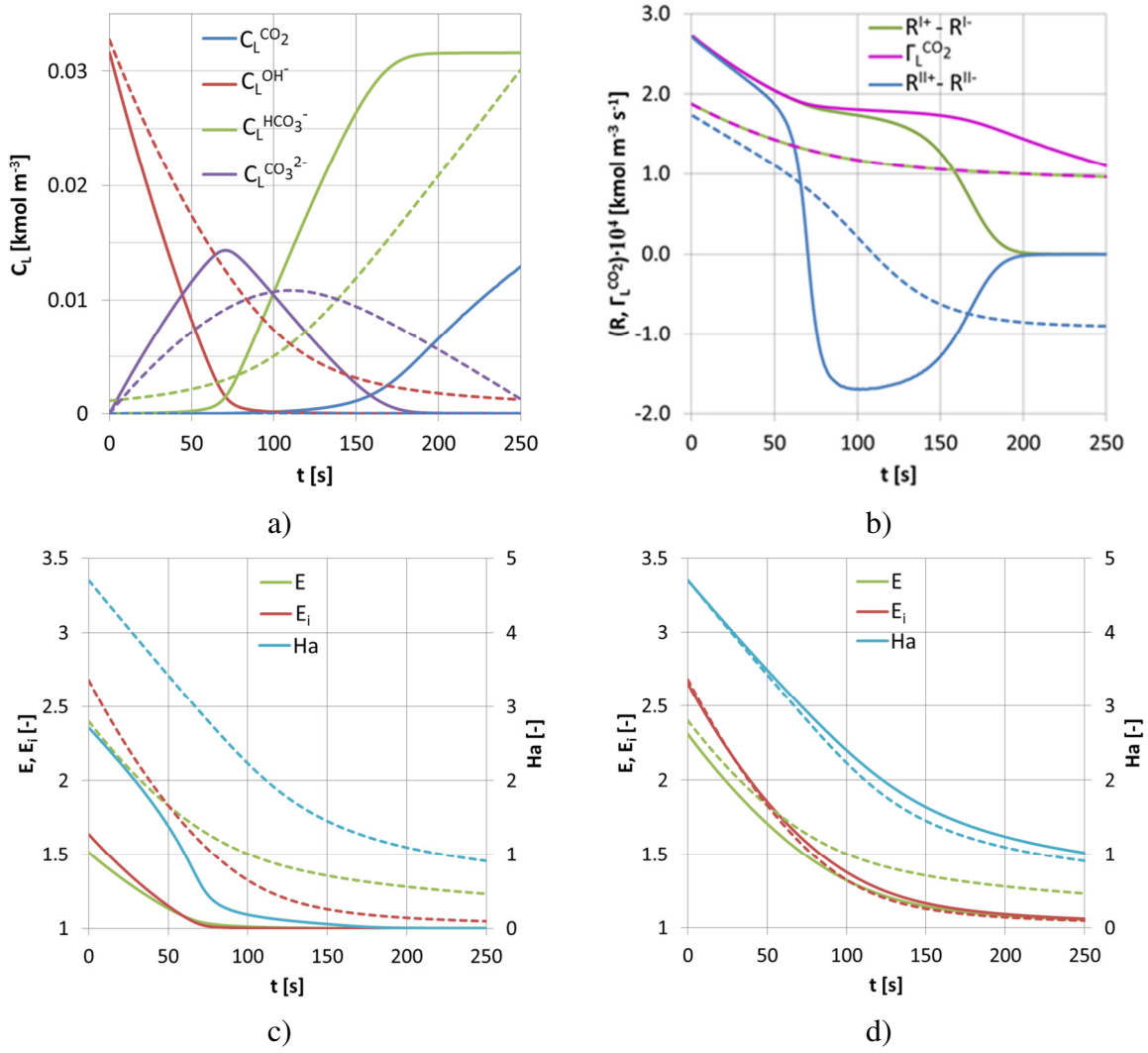

Figure 9: Effect of adding carbonate ions with a concentration of 1 kmol m^{-3} to the initial solution. Comparison of results obtained from the simplified pointwise calculation. Parts a)-c) compare cases with (dashed lines) and without (solid lines) initial carbonate ions using enhancement factor model 2A showing time-dependent species concentrations, time-dependent effective reaction and absorption rates, and time-dependent enhancement factors and Hatta number, respectively. Note that the curve for $C_L^{CO_3^{2-}}$ in part a) gives the difference to the initial concentration. Part d) compares results for enhancement factor models 1C (solid lines) and 2A (dashed lines) for the case with initial carbonate ions. Only the time-dependent enhancement factors and Hatta number are shown.

4.4 Effect of an increased temperature

As already mentioned above, an increase in temperature causes a decrease of the equilibrium constant K^{II} whereby the second backward reaction gains a more pronounced influence on the enhancement. The resulting effects are demonstrated in Fig. 10. A moderate increase in the

temperature to 50°C over the previous value of 25°C already gave a notable change in the results. In addition to shifting the equilibrium of the second reaction, this also increases the forward rate constant of reaction I by a factor of almost 4, decreases the CO_2 solubility by ~33% and increases the CO_2 diffusivity by ~75%. Again, all of these effects act together. The density and molecular viscosity of pure water at 50°C are 988 kg m^{-3} and 0.547 mPa s.

Fig. 10a) shows a comparison of the species concentrations for the cases with process temperatures of 50°C (dashed lines) and 25°C (solid lines) calculated using the enhancement factor model 2A which is appropriate for the two-step reaction. It can be seen that the effect on the species concentrations is not as big as that of the initial addition of 1 kmol m^{-3} of sodium carbonate discussed in the preceding section and the overall temporal evolution remains more similar. In the initial stage of the process some bicarbonate is obtained and the peak in the carbonate concentration is a bit lower if the temperature is increased.

These findings are in accordance with the difference between the effective rates of reactions I and II being somewhat larger for the case with higher temperature as shown in Fig. 10b). In the initial stage of the process the absorption rates for both cases are almost the same despite the lower solubility at the higher temperature. This can be explained by a compensating increase in the mass transfer coefficient due to the higher diffusivity as well as the larger enhancement factor (see Fig. 10d). At later times where the enhancement effect has ceased, smaller gas absorption rates due to reduced CO_2 solubility are clearly visible in Fig. 10b). As before, peaks in the maximum carbonate concentration coincide with zero crossings of the effective rate of reaction II.

From Fig. 10d) it is seen that when the temperature is increased the Hatta number becomes larger, which is caused by both the increased rate constant of reaction I and the increased diffusivity of CO_2. Correspondingly a larger value of the enhancement factor is expected for the case with increased temperature. For this case, the value of E is even higher than that of E_i throughout the monitoring period. This is caused by the higher value of E_i' which again points to the importance of the two-step nature of the reaction.

To further quantify the error that incurs for the simpler one-step models the time-dependent pH-value, which is easily measurable, is considered in Fig. 10c). The calculation result using model 1C (dash-dotted line) gives higher values than obtained for model 2A (dashed line) for the temperature of 50°C. Compared with the difference to the case with 25°C temperature this overprediction amounts to 25 … 30%.

In summary, the results by adding sodium carbonate to the initial solution or increasing the temperature demonstrate that under certain circumstances, a two-step enhancement factor model is appropriate for the CO_2/NaOH system. In general, the choice of a one-step model is justified if throughout the entire time span during which enhancement occurs, the effective rate of the consecutive reaction remains positive and is of the same order of magnitude as the effective rate of reaction I. Under this condition, all bicarbonate will be converted to carbonate. Since this is true for the case of Darmana et al. (2007), the enhancement factor model for a one-step reaction based on the renewal model Eq. (17) together with the fit formula for the instantaneous limit Eqs. (B.4-B.6) will be used for the final investigation concerning the importance of the water pathway Eq. (8).

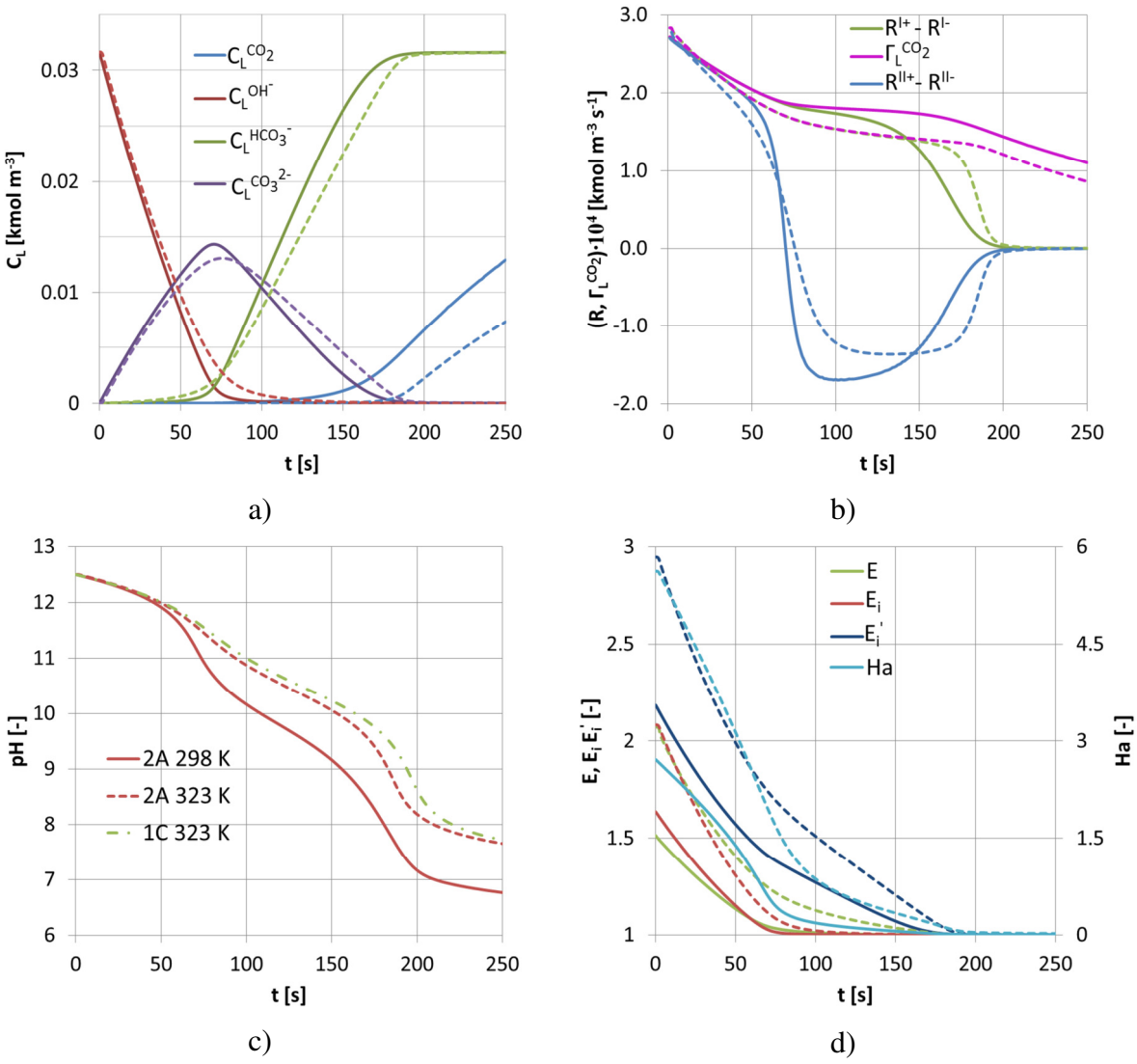

Figure 10: Effect of increasing temperature from 25°C (solid lines) to 50°C (dashed lines) using enhancement factor model 2A. Comparison of results obtained from the simplified pointwise calculation: a) time-dependent species concentrations, b) time-dependent effective reaction and absorption rates c) time-dependent pH-value, d) time-dependent enhancement factors and Hatta number. Part c) in addition includes the result using one-step enhancement factor model 1C (dash-dotted lines) at 50°C for comparison.

4.5 Inclusion of the water pathway

The discussion so far has ignored the water pathway, i.e. reaction III, in the reaction model of section 3, which becomes relevant at pH-values below 10. If this is taken into account, the results can be further improved as shown in Fig. 11, comparing cases with the water pathway included (smooth solid lines) or neglected (dash-dotted lines). It should be noted that reaction III is too slow to cause an enhancement of mass transfer. The enhancement due to reaction I is described by model 1C for the present purpose.

Up to a time of about 100 s no differences are observable between both cases. For the pH-value in Fig. 11a), the steep drop occurring at ~ 150s in the experimental data (noisy solid line) can also be observed in the model calculations upon including the water pathway. It still

sets in a bit later than in the experiment, but the shape of the curve is improved substantially. In the other species concentrations in Fig. 11c), only small differences are visible between 150 and 200 s. The enhancement factor in Fig. 11b) is unaffected by the change, because the enhancement effect has already ceased at a much earlier stage of the process. Also only tiny differences are seen in the Hatta number.

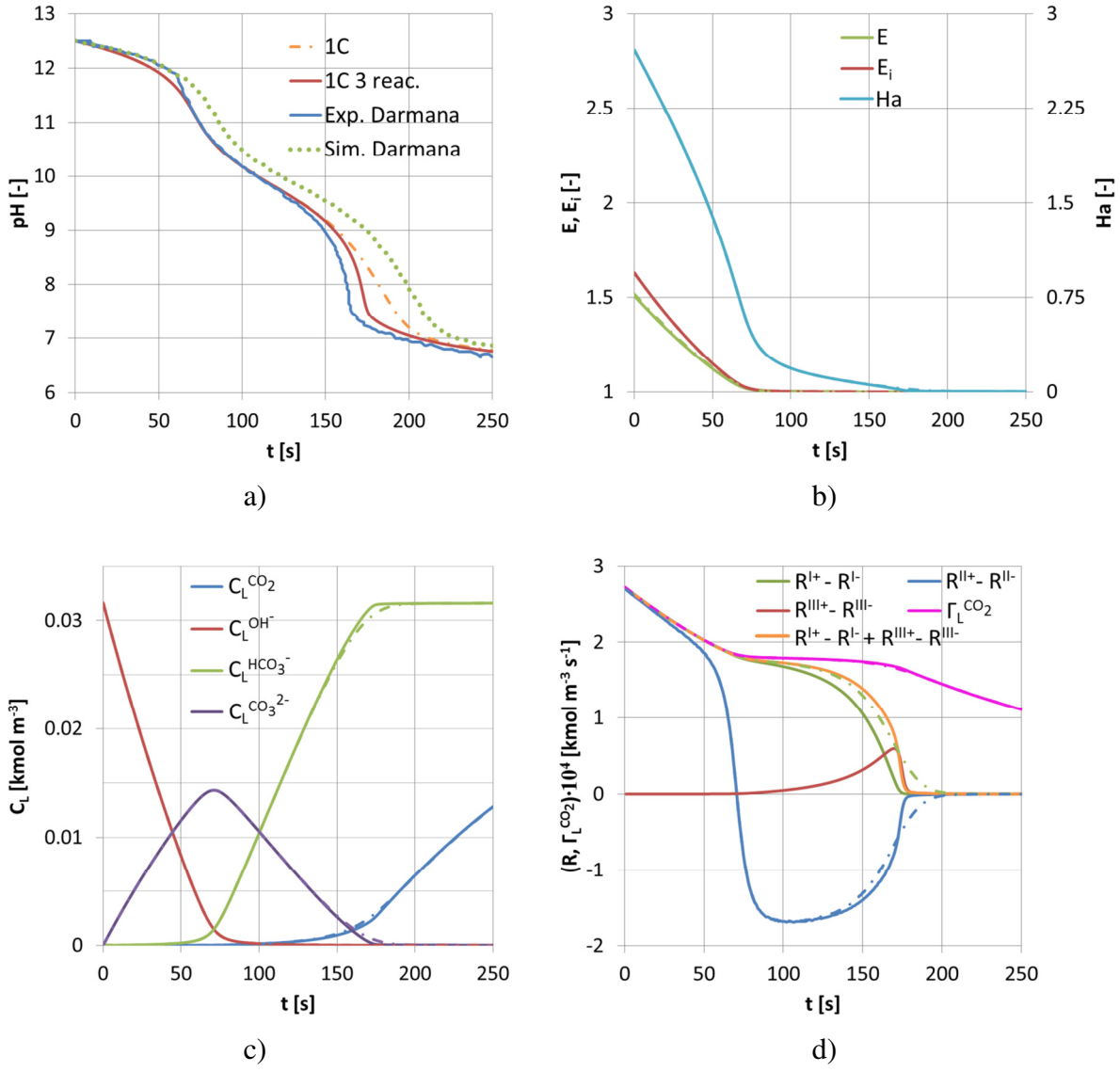

Figure 11: Comparison of results with the water pathway included (smooth solid lines) or neglected (dash-dotted lines) for the enhancement factor model 1C: a) time-dependent pH-value, with Euler-Lagrange simulations of Darmana et al. (2007) (thick dots) and measured values of Darmana et al. (2007) (noisy solid line) shown again for comparison, b) Time-dependent enhancement factors and Hatta number, c) time-dependent species concentrations, d) time-dependent effective reaction and absorption rates.

The effective rate of reaction III in Fig. 11 d) clearly shows that the water pathway becomes important if the pH-value falls below 10, which occurs at t ≈ 100 s. As the pH-value further decreases below a value of 8, which occurs at t ≈ 170 s, reaction III prevails over reaction I. It

is notable that along with the increase in the rate of reaction III, the rate of reaction I becomes smaller than for the case without the water pathway. This is due to the consumption of aqueous CO_2 by reaction III. In fact, the sum of the effective rates of reactions I and III, which gives the total consumption of CO_2, is close to the effective rate of reaction I, when the water pathway is neglected. However, in the range from ~130 … 170 s a slightly higher consumption of CO_2 is visible if the water pathway is included, which finally leads to the faster decrease in pH-value. Furthermore, the backward reaction II proceeds a bit faster, resulting in the slightly faster decrease in carbonate concentration and the slightly faster increase in bicarbonate concentration seen in Fig. 11c).

5 CONCLUSIONS AND OUTLOOK

The reactive absorption of CO_2 into aqueous NaOH in a bubble column has been analysed by means of a simplified treatment looking only at a single measurement point. Experimental data of Darmana et al. (2007) were used to compare different enhancement factor models for this reaction. By substituting values from the experiment to determine the mass transfer coefficient and interfacial area concentration, possible inaccuracies from the fluid-dynamic part of a more complete model were avoided. The validity of this simplified approach was assured by comparison with Euler-Lagrange simulation results also given by Darmana et al. (2007).

The comparison between different enhancement factor models showed that approximate expressions for the enhancement of an instantaneous second order reaction that appear frequently in reaction engineering textbooks should be considered with care. A fit formula was presented that gives much better accuracy. Making use of this formula, expressions derived from renewal, penetration, and film models agree with each other rather well. The two-step nature of the reaction system did not play a significant role for the conditions of the experiment of Darmana et al. (2007). However, its consequences may be notable if additional carbonate is present initially or the temperature is increased. Detailed examples have been presented to guide the design of future experiments, where effects of the two-step reaction can be observed.

However, consideration of the reaction between CO_2 and water was found essential to capture the behaviour at lower pH-values as the neutral point is approached. Good agreement with the experimental data was reached once this additional reaction pathway was included in addition to the reaction between CO_2 and hydroxide ions. A full model for the reaction kinetics involving both pathways and the subsequent carbonate-bicarbonate equilibrium was given.

After the proper modeling of the reaction and the resulting enhancement of the mass transfer has now been ascertained, the next step is to integrate this into a full multiphase CFD simulation. This will be presented in a sequel paper using a previously validated Euler-Euler model for fluid-dynamics and mass transfer in bubbly flows (Rzehak and Krepper, 2013 and 2015; Rzehak and Kriebitzsch, 2015; Rzehak and Krepper, 2016).

6 ACKNOWLEDGEMENT

This work has been carried out in the frame of a research project (GZ: RZ 11/1-1) within the DFG Priority Programme 1740: “Reactive Bubbly Flows” funded by the DFG.

7 APPENDIX A: REACTION AND MATERIAL MODEL

A model for the kinetics of the reaction Eqs. (10) - (15), as well as diffusivity and solubility of the reactants, which contains the dependence on temperature and ionic effects as much as available from the literature, is presented in the following. The development extends the model proposed by Darmana et al. (2007) and offers some further discussion. Compared with the original references from which the correlations have been taken, some adjustments have been made to obtain consistent units and a sensible number of significant digits in numerical parameter values.

7.1 Solubility

Under the condition of low solute concentration, the solubility of CO_2 in water is described by a Henry constant *He*. From different definitions in use, the dimensionless ratio of the concentration in the liquid to the concentration in the gas at equilibrium is the most convenient for the present purpose. A correlation for the temperature-dependence in pure water has been given by Versteeg and van Swaaij (1988) based on own measurements as

$$He_W^{CO_2} = 3.54 \cdot 10^{-7} RT \exp\left(\frac{2044[K]}{T}\right) \cdot \left[mol\ J^{-1}\right]. \qquad \text{(A.1)}$$

A more complex expression has been given in a comprehensive literature review by Crovetto (1991) for which validity up to P = 1 MPa has been ascertained. Since deviations between both are restricted to T close to 0°C the simpler expression Eq. (A.1) has been used herein following Rzehak and Krepper (2016).

Due to the salting-out effect in electrolytic solutions, the solubility of most gases is decreasing with increasing salt concentration. Weisenberger and Schumpe (1996) presented a method which is able to predict the solubility of different gases in different salt solutions by extension of a model developed by Schumpe (1993). The resulting expression is

$$He^{CO_2} = He_W^{CO_2} 10\text{^}\left(-\sum\left(h^I + h^A\right) C_L^I\right), \qquad \text{(A.2)}$$

where $h^A = h_0^A + h_T^A\left(T - 298.15\ [K]\right)$. The required constants for the present system are given in table A.1. For the case of Darmana et al. (2007), application of Eq. (A.2) to include the ionic effects leads to a maximum decrease of 1.5 % in solubility of CO_2 compared to its solubility in pure water. For other conditions such as the case with added carbonate considered in section 4.3, the ionic effect may be about 50 %.

Ion	h^I [m^3 kmol^{-1}]	Gas	h_0^A [m^3 kmol^{-1}]	h_T^A [m^3 kmol^{-1} K^{-1}]
Na^+	0.1143	CO_2	-0.0172	$-0.338 \cdot 10^{-3}$
OH^-	0.0839			
HCO_3^-	0.0967			
CO_3^{2-}	0.1423			

Table A.1: Parameters for Eq. (A.2).

7.2 Diffusivity

The temperature dependence of the molecular diffusivity of CO_2 in water has also been correlated by Versteeg and van Swaaij (1988) based on a review of earlier literature data as

$$D_W^{CO_2} = 2.35 \cdot 10^{-6} \exp\left(\frac{-2119\ [K]}{T}\right) \cdot \left[m^2 s^{-1}\right]. \tag{A.3}$$

More recent data have been provided by Frank et al. (1996) which match Eq. (A.3) as well. All of these data have been taken at atmospheric pressure. Data of Lu et al. (2013) at P = 20 MPa still fall within the scatter of the atmospheric pressure values. Since all data match very well with the correlation Eq. (A.3), this is adopted for the present work again following Rzehak and Krepper (2016).
The molecular diffusivity of CO_2 in electrolytic solutions containing relatively small ions in moderate concentrations can be calculated with a method suggested by Ratcliff and Holdcroft (1963) as

$$D^{CO_2} = D_W^{CO_2}\left(1 + 0.624 \sum b^I C_L^I\right). \tag{A.4}$$

The required constants b^I are shown in Table A.2. For the case of Darmana et al. (2007), the decrease in the diffusivity of CO_2 with respect to its diffusivity in pure water due to this ionic effect is less than 0.5 %. When higher concentrations are involved as in the example discussed in section 4.3, the effect can be in the range of 25%.

Ion	b^I [m^3 kmol^{-1}]
Na^+	-0.0857
OH^-	-0.1088
HCO_3^-	-0.1150
CO_3^{2-}	-0.2450

Table A.2: Parameters for Eq. (A.4).

The temperature dependent molecular diffusion coefficients of the other species in solution are determined by power-law fits of the type

$$D^I = D_0^I \left(\frac{T}{T^I} - 1\right)^{\gamma^I} \tag{A.5}$$

as suggested by Zeebe (2011). The constants D_0^I, T^I, and γ^I are given in table A.3. For bicarbonate and carbonate ions these have been found by Zeebe (2011) from fits to molecular dynamics simulation results. The constants for the sodium ion are obtained by fitting them to the results of a molecular dynamics simulation of Bastug and Kuyucak (2005). The constants for the diffusivity coefficient of hydroxide ions are based on the conductivity measurements of Light et al. (2005). The simulations of Zeebe (2011) and experiments of Light et al. (2005) were performed at infinite dilution. Bastug and Kuyucak (2005) performed their simulations for a 0.1 M solution, but give a comparison with experimental data which suggests that the results are also applicable at infinite dilution.

Ion	$D_0^I \cdot 10^9$ [m^2 s^{-1}]	T^I [K]	γ^I [-]
Na^+	5.391	209.7	1.619
OH^-	26.65	216.5	1.658
HCO_3^-	7.016	204.0	2.394
CO_3^{2-}	5.447	210.3	2.193

Table A.3: Parameters for Eq. (A.5).

7.3 Reaction Rate constants

The rate constant of the first forward reaction (Eq. (5)) was investigated by Pohorecki and Moniuk (1988) using a laminar jet technique. They found that it depends on ionic strength and temperature as

$$k_L^{I+} = k_L^{I+,\infty} 10\text{^}\left(0.221 \ \frac{I}{[kmol\ m^{-3}]} - 0.016 \ \frac{I^2}{[kmol^2 m^{-6}]} \right), \tag{A.6}$$

where the temperature dependent rate constant at infinite dilution of ions, $k_L^{I+,\infty}$, is given by

$$k_L^{I+,\infty} = 10\text{^}\left(-\frac{2382\ [K]}{T} + 11.90 \right) \text{[m}^3 \text{ kmol}^{-1} \text{ s}^{-1}\text{]}. \tag{A.7}$$

The ionic strength I is defined in terms of the concentration and the valency z of the dissolved ions

$$I = \frac{1}{2}(C_L^{Na^+} z_{Na^+}^2 + C_L^{OH^-} z_{OH^-}^2 + C_L^{HCO_3^-} z_{HCO_3^-}^2 + C_L^{CO_3^{2-}} z_{CO_3^{2-}}^2). \tag{A.8}$$

Since reaction I plays a role only for pH $\geq$ 8, at which the concentration of H+ ions is hundered times lower than that of OH- ions, the former have been neglected in this expression. For the case of Darmana et al. (2007), the first forward reaction rate constant may be increased by a maximum of 2.5 % due to this ionic effect described by Eqs. (A.6) and (A.8). For other conditions such as the case with added carbonate considered in section 4.3, the ionic effect may be a factor of 3.

Pohorecki and Moniuk (1988) also offer a more refined consideration of reaction I in mixed electrolyte systems showing that each ionic species ought to appear with an individual coefficient in the reaction rate, rather than lumped together in terms of the ionic strength. However, the coefficient for one important ion species, namely HCO_3^-, was not determined in their work, so that unfortunately their refined model cannot be used for the present purpose.

The first reaction, Eq. (5), is coupled with the third one, Eq. (8) by the auto-dissociation of water. Therefore the equilibrium constant K^W of the ionization of water is needed. Tsonopoulos et al. (1976) proposed an equation describing the temperature dependence of K_W as

$$K_W = C_L^{H^+} C_L^{OH^-} = 10\text{^}\left(-\frac{5840\ [K]}{T} + 55.2062 - 22.48\ \lg\left(\frac{T}{[K]}\right)\right) \cdot [kmol^2\ kg^{-2}] \cdot \left(\rho^{H_2O}(T)\right)^2 \cdot \quad \text{(A.9)}$$

Considering the equilibrium constant K^{III} of reaction III (Eq. (8)), which is determined from a relation found by Edwards et al. (1978)

$$K_L^{III} = \frac{C_L^{HCO_3^-} C_L^{H^+}}{C_L^{CO_2}} = \exp\left(\frac{-12090\ [K]}{T} + 235.5 - 36.78\ \ln\left(\frac{T}{[K]}\right)\right) \cdot 10^{-3} \cdot [kmol\ kg^{-1}] \cdot \rho^{H_2O}(T), \quad \text{(A.10)}$$

the backward reaction rate constant of reaction I (Eq. (5)) is obtained as

$$k_L^{I-} = \frac{K^W}{K_L^{III}} k_L^{I+}. \quad \text{(A.11)}$$

It should be mentioned that for higher concentrations, K^{III} also depends significantly on ionic strength (Millero et al., 2006; Zeebe and Wolf-Gladrow, 2001; Johnson, 1982; Knoche, 1980) which corresponds with the ionic nature of the backward reaction of reaction III (Eq. (8)).

The forward reaction rate constant k_L^{II+} of the second reaction (Eq. (6)) is in the order of $10^{10}\ldots10^{11}$ m^3 kmol^{-1} s^{-1} as determined by Eigen (1954). This extremely high reaction rate constant is due to the fact that only a proton transfer occurs. As shown by Darmana et al. (2007) a significantly smaller value can be used as long as this reaction remains much faster than all others, most importantly $k_L^{II+} >> k_L^{I+}$. We have determined that even with $k_L^{II+} = 10^4$ m^3 kmol^{-1} s^{-1} there is negligible influence on the results.

As suggested by Hikita et al. (1976), the equilibrium constant K^{II} of the second reaction considering dependence on the sodium concentration is determined as

$$K_L^{II} = \frac{C_L^{CO_3^{2-}}}{C_L^{OH^-} C_L^{HCO_3^-}} = K_L^{II,\infty} 10\text{^}\left(\frac{1.01 \sqrt{\frac{C_L^{Na^+}}{[kmol\ m^{-3}]}}}{1+1.27 \sqrt{\frac{C_L^{Na^+}}{[kmol\ m^{-3}]}}} + 0.125\ \frac{C_L^{Na^+}}{[kmol\ m^{-3}]} \right), \quad \text{(A.12)}$$

where

$$K_L^{II,\infty} = 10\text{^}\left(\frac{1567\ [K]}{T} + 0.4134 - 0.006737 \frac{T}{[K]} \right) \left[kmol^{-1} m^3\right] \quad \text{(A.13)}$$

is the temperature dependent rate at infinite dilution of sodium ions.

The backward reaction rate constant k_L^{II-} then is calculated from

$$k_L^{II-} = \frac{k_L^{II+}}{K_L^{II}}. \quad \text{(A.14)}$$

Since only uncharged molecules are involved in the third forward reaction (Eq. (8)) the reaction rate constant k_L^{III+} depends on temperature but not ionic strength. According to Johnson (1982) it can be determined as

$$k_L^{III+} = \exp\left(-\frac{6.19 \cdot 10^4 [K]}{T} + 1247 - 183 \ln\left(\frac{T}{[K]} \right) \right). \tag{A.15}$$

The backward reaction rate constant k_L^{III-} is calculated with the aid of the previously introduced equilibrium constant K^{III} (Eq. (A.10))

$$k_L^{III-} = \frac{k_L^{III+}}{K_L^{III}}. \tag{A.16}$$

8 APPENDIX B: FIT FORMULA FOR THE ENHANCEMENT FACTOR OF AN INSTANTANEOUS ONE-STEP REACTION OF SECOND-ORDER

As described in section 3.2, the solution of the penetration model for an instantaneous second order reaction results in an implicit expression, Eq. (20), for the enhancement factor E_i. This expression contains two parameters,

$$\chi = \frac{C_{L,\infty}^{B}}{\nu^{B} C_{L,I}^{A}} \sqrt{\frac{D_L^B}{D_L^A}} \tag{B.1}$$

and

$$\delta = \sqrt{\frac{D_L^B}{D_L^A}}\,. \tag{B.2}$$

The numerical evaluation of Eq. (20) shown as the solid lines in Fig. 4b) reveals for both small and large values of the parameter χ a linear dependence

$$E_i = 1 + slope\ \chi\,, \tag{B.3}$$

which manifests itself as straight lines with slope one on the log-log plot. Values of the slope determined for small values of the parameter χ are shown in Fig. B.1 as a function of $1/\delta$. It may be seen that the slope is close, although not exactly equal, to $1/\delta$.

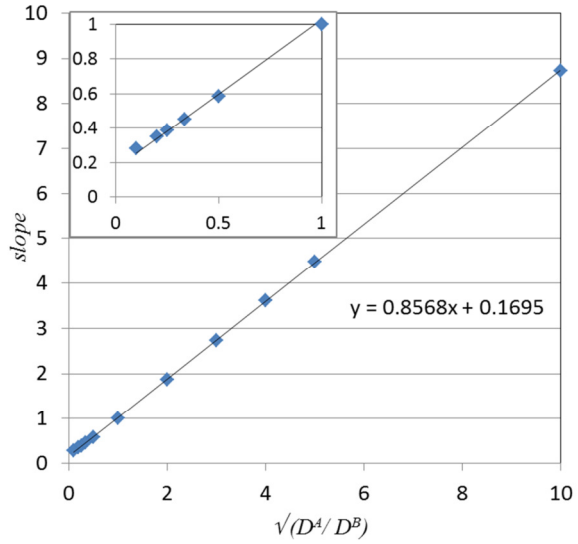

Figure B.1: Slope in Eq. (B.3) determined from the numerical evaluation of Eq. (20) for small values of χ. The inset shows an enlarged view of the region near the origin.

Based on these observations a fit is sought for $(E_i - 1)\ \delta/\chi$. The result for $\delta > 1$ is

$$(E_i - 1)\frac{\delta}{\chi} = 1 + \frac{1}{2}(\delta - 1)\left(\frac{2}{\pi}\arctan\left(0.2\frac{\pi}{2}\ln(\exp(\chi) - 1)\right) + 1\right), \tag{B.4}$$

while for $\delta < 1$

$$(E_i - 1)\frac{\delta}{\chi} = 1 + \frac{1}{2}(\delta - 1)\left(\frac{2}{\pi}\arctan\left(0.2\frac{\pi}{2}\ln\left(\exp\left(\frac{\chi}{\sqrt{\delta}}\right) - 1\right)\right) + 1\right). \qquad \text{(B.5)}$$

Note that for δ = 1 both expressions give the same value

$$(E_i - 1)\frac{\delta}{\chi} = 1, \qquad \text{(B.6)}$$

which coincides with the exact result Eq. (21) for this case.
Here, the function $\ln(\exp(x) - 1)$ maps its arguments, which are always positive, to the entire real line. The function $\frac{2}{\pi}\arctan(\alpha\frac{\pi}{2}x)$ then maps the real line to the finite interval [-1,1], which is finally shifted and scaled to the desired range between 1 for small χ and δ for large χ. The appearance of $\sqrt{\delta}$ in the innermost argument in Eq. (B.5) and the value of $\alpha = 0.2$ were found by trial and error.
The fit formula for $(E_i - 1)\ \delta/\chi$ is compared to results from the numerical evaluation of Eq. (20) in Fig. B.2. A comparison for the final results on E_i has been shown in Fig. 4. Within a fairly wide range of parameter values, namely

$$0.01 \le \frac{C^B_{L,\infty}}{\nu^B C^A_{L,I}}\sqrt{\frac{D^B_L}{D^A_L}} \le 100 \qquad \textit{and} \qquad 0.01 \le \frac{D^B_L}{D^A_L} \le 100, \qquad \text{(B.7)}$$

the relative deviation between the fit formula and the numerical evaluation of Eq. (20) for E_i is no more than 20%.

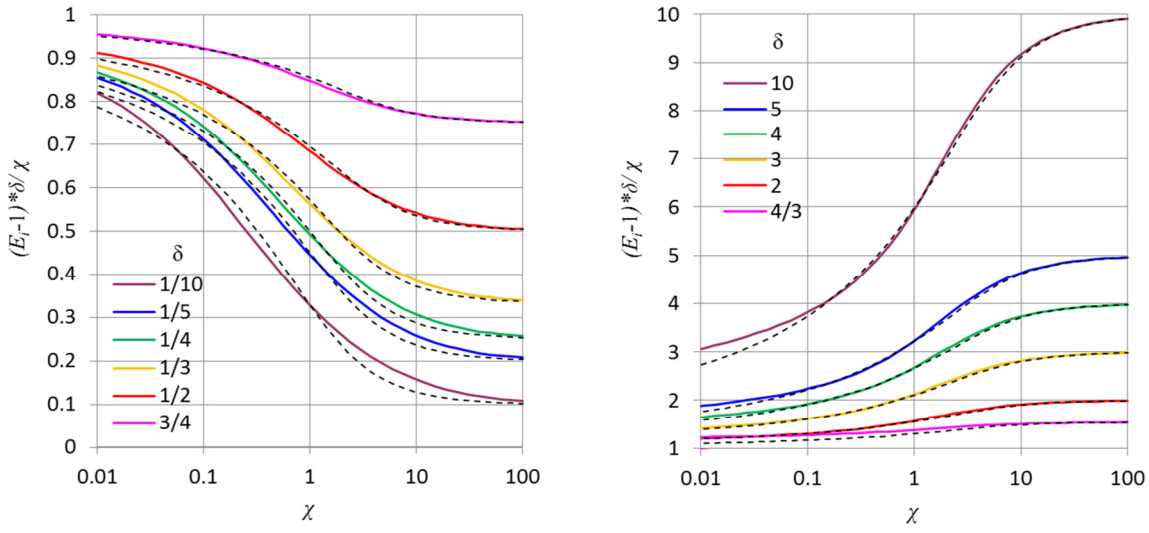

Figure B.2: Comparison of fit formula for $(E_i - 1)\ \delta/\chi$, Eqs. (B.4) – (B.6) (dashed lines) with results from numerical evaluation of Eq. (20) (solid lines).

9 NOMENCLATURE

Notation	Unit	Denomination
a_I	m^{-1}	interfacial area concentration
C_L	kmol m^{-3}	molecular species concentration in the bulk liquid
d_B	m	bubble diameter
D^X	m^2 s^{-1}	diffusion coefficient of species X
E	-	enhancement factor
Ha	-	Hatta number
He	-	Henry constant
I	kmol m^{-3}	ionic strength
J_L	m s^{-1}	liquid volumetric flux = superficial velocity
$k_L^{\Xi\pm}$	$(m^3\ kmol^{-1})^{\xi-1}$ s^{-1}	for- (+) and backward (-) rate constant of reaction Ξ with total reaction order ξ
k_L	m s^{-1}	mass transfer coefficient
K_L^{Ξ}	$(m^3\ kmol^{-1})^{\xi^+-\xi^-}$	equilibrium constant of reaction Ξ with total reaction orders $\xi^{\pm}$ for- (+) and backward (-) reaction
K_W	$kmol^2$ m^{-6}	ionization constant of water
M	kg $kmol^{-1}$	molar mass
Mo	-	Morton Number
P	Pa = N m^{-2}	pressure
$R_L^{\Xi\pm}$	kmol m^{-3} s^{-1}	for- (+) and backward (-) rate of reaction Ξ
Re	-	Reynolds number
S	kg m^{-3} s^{-1}	mass source due to reactions
Sc	-	Schmidt number
T	K	temperature
u_{rel}	m s^{-1}	relative velocity
X	-	mole fraction
Y	-	mass fraction
z	-	valency
α	-	phase fraction
Γ	kg m^{-3} s^{-1}	mass source due to absorption
μ	m^2 s^{-1}	dynamic viscosity
ρ	kg m^{-3}	density

Subscript	Denomination
B	bubble
G	gas phase
i	instantaneous
I	phase interface
L	liquid phase
W	pure water
∞	bulk of liquid phase

Superscript	Denomination
I	first reaction (Eq. (5))
II	second reaction (Eq. (6))
III	third reaction (Eq. (8))
+	forward reaction
-	backward reaction

10 REFERENCES

Bastug, T. and Kuyucak, S., 2005. Temperature dependence of the transport coefficients of ions from molecular dynamics simulations. *Chemical Physics Letters* 408, 84–88.

Bauer, M. and Eigenberger, G., 2000. Multiscale modeling of hydrodynamics, mass transfer and reaction for CO2 chemisorption in bubble column reactors. *16th International Association for Mathematics and Computers in Simulation (IMACS) World Congress*, Lausanne, Swizzerland.

Becker, S., 1996. Experimentelle Untersuchungen von Blasensäulen als Basis für detaillierte Modellrechnungen. *Universität Stuttgart*, Ph. D. thesis (in German).

Bird, R. B., Stewart, W. E., and Lightfoot, E. N., 2002. Transport Phenomena. *Wiley*, 2nd ed.

Brauer, H., 1981. Particle/fluid transport processes. *Progress in Chemical Engineering* 19, 81–111.

Brian, P. L. T., Hurley, J. F. and Hasseltine, E. H., 1961. Penetration Theory for Gas Absorption Accompanied by a Second Order Chemical Reaction. *AlChE Journal* 7, 226–231.

Chang, C. S. and Rochelle, G. T., 1982. Mass transfer enhanced by equilibrium reactions. *Ind. Eng. Chem. Fundamen.* 21, 379–385.

Clift, R., Grace, J. R. and Weber, M. E., 1978. Bubbles, drops, and particles. *Academic Press*.

Cockx, A., Do-Quang, Z., Audic, J., Line, A. and Roustan, M., 2001. Global and local mass transfer coefficients in waste water treatment process by computational fluid dynamics. *Chemical Engineering and Processing: Process Intensification* 40, 187–194.

Couchaux, G., Barth, D., Jacquin, M., Faraj, A., and Grandjean, J., 2014. Kinetics of Carbon Dioxide with Amines I. Stopped-Flow Studies in Aqueous Solutions: A Review. *Oil & Gas Science and Technology* 69, 865–884.

Crovetto, R., 1991. Evaluation of Solubility Data of the System CO2–H2O from 273 K to the Critical Point of Water. *Journal of Physical and Chemical Reference Data* 20, 575–589.

Cussler, E. L., 2007. Diffusion - Mass transfer in liquid systems. *Cambridge University Press*, 3rd ed.

Danckwerts, P. V., 1970. Gas-liquid reactions. *McGraw-Hill.*

Darmana, D., Henket, R., Deen, N. and Kuipers, J., 2007. Detailed modelling of hydrodynamics, mass transfer and chemical reactions in a bubble column using a discrete bubble model: Chemisorption of CO2 into NaOH solution, numerical and experimental study. *Chemical Engineering Science* 62, 2556–2575.

DeCoursey, W. J., 1974. Absorption With Chemical Reaction: Development Of A New Relation For The Danckwerts Model. *Chemical Engineering Science* 29, 1867–1872.

Edwards, T. J., Maurer, G., Newman, J. and Prausnitz, J. M., 1978. Vapor-Liquid Equilibria in Multicomponent Aqueous Solutions of Volatile Weak Electrolytes. *AlChE Journal* 24, 966–976.

Eigen, M., 1954. Methods For Investigation Of Ionic Reactions In Aqueous Solutions With Half-times As Short As 10^-9 Sec: Application To Neutralization And Hydrolysis Reactions. *Discussions of the Faraday Society* 17, 194–205.

Eigen, M., Kustin, K. and Maass, G., 1961. Die Geschwindigkeit der Hydratation von SO2 in wäßriger Lösung. *Zeitschrift für Physikalische Chemie* 30, 130–136.

Eigen, M., 1964. Proton Transfer, Acid-Base Catalysis, and Enzymatic Hydrolysis. Part I: Elementary Processes. *Angew. Chem. Int. Ed. Engl.* 3, 1–19.

Feron, P. (Ed.), 2016. Absorption-Based Post-combustion Capture of Carbon Dioxide. *Elsevier.*

Fleischer, C., Becker, S. and Eigenberger, G., 1996. Detailed Modeling Of The Chemisorption Of CO2 Into NaOH In A Bubble Column. *Chemical Engineering Science* 51, 1715–1724.

Frank, M. J. W., Kuipers, J. A. M., and van Swaaij, W. P. M., 1996. Diffusion Coefficients and Viscosities of CO2+H2O, CO2+CH3OH, NH3+H2O, and NH3+CH3OH Liquid Mixtures. *Journal of Chemical & Engineering Data* 41, 297–302.

Glasscock, D. A. and Rochelle, G. T., 1989. Numerical Simulation of Theories for Gas Absorption with Chemical Reaction. *AIChE Journal* 35, 1271–1281.

Gruber, M. C., Radl, S. and Khinast, J. G., 2015. Rigorous modeling of CO2 absorption and chemisorption: The influence of bubble coalescence and breakage. *Chemical Engineering Science* 137, 188–204.

Hikita, H. and Asai, S., 1964. Gas absorption with (m,n)-th order irreversible chemical reaction. *International Chemical Engineering* 4, 332–340.

Hikita, H., Asai, S. and Takatsuka, T., 1976. Absorption of carbon dioxide into aqueous sodium hydroxide and sodium carbonate-bicarbonate solutions. *The Chemical Engineering Journal* 11, 131–141.

Hikita, H. and Asai, S., 1976a. Gas Absorption with a Two-step Chemical Reaction. *The Chemical Engineering Journal* 11, 123–129.

Jain, D., Kuipers, J. A. M., and Deen, N. G., 2015. Numerical modeling of carbon dioxide chemisorption in sodium hydroxide solution in a micro-structured bubble column *Chemical Engineering Science* 137, 685–696.

Jeffrey, A., 2005. Mathematics for engineers and scientists. *Chapman & Hall*, 6th ed.

Johnson, K. S., 1982. Carbon dioxide hydration and dehydration kinetics in seawater. *Limnology and Oceanography* 27, 849–855.

Kern, D. M., 1960. The hydration of carbon dioxide. *Journal of Chemical Education* 37, 14–23.

Knoche, W., 1980. Chemical Reactions of CO2 in Water. *Biophysics and Physiology of Carbon Dioxide*, *Springer*, 3–11.

Kohl, A. L. and Nielsen, R. B., 1997. Gas Purification. *Elsevier.*

Kucka, L., Müller, I., Kenig, E. Y. and Gorak, A., 2003. On the modelling and simulation of sour gas absorption by aqueous amine solutions. *Chemical Engineering Science* 58, 3571–3578.

Light, T. S., Licht, S., Bevilacqua, A. C. and Morash, K. R., 2005. The Fundamental Conductivity and Resistivity of Water. *Electrochemical and Solid-State Letters* 8, E16–E19.

Lu, W., Guo, H., Chou, I., Burruss, R., and Li, L., 2013. Determination of diffusion coefficients of carbon dioxide in water between 268 and 473 K in a high-pressure capillary optical cell with in situ Raman spectroscopic measurements. *Geochimica et Cosmochimica Acta* 115, 183–204.

Mandal, B. P., Guha, M., Biswas, A. K., and Bandyopadhyay, S. S., 2001. Removal of carbon dioxide by absorption in mixed amines: modelling of absorption in aqueous MDEA/MEA and AMP/MEA solutions. *Chemical Engineering Science* 56, 6217–6224.

Marquez, M. A., Amend, R. J., Carbonell, R. G., Saez, A. E., and Roberts, G. W., 1999. Hydrodynamics of gas-lift reactors with a fast, liquid-phase reaction. *Chemical Engineering Science* 54, 2263–2271.

Millero, F. J., Graham, T. B., Huang, F., Bustos-Serrano, H. and Pierrot, D., 2006. Dissociation constants of carbonic acid in seawater as a function of salinity and temperature. *Marine Chemistry* 100, 80–94.

Olander, D. R., 1960. Simultaneous mass transfer and equilibrium chemical reaction. *AIChE Journal* 6, 233–239.

Pacheco, M. A. and Rochelle, G. T., 1998. Rate-Based Modeling of Reactive Absorption of CO2 and H2S into Aqueous Methyldiethanolamine. *Ind. Eng. Chem. Res.* 37, 4107–4117.

Pinsent, B. R. W., Pearson, L. and Roughton, F. J. W., 1956. The kinetics of combination of carbon dioxide with hydroxide ions. *Trans. Faraday Soc.* 52, 1512–1520.

Pohorecki, R. and Moniuk, W., 1988. Kinetics of Reaction Between Carbon Dioxide and Hydroxyl Ions in Aqueous Electrolyte Solutions. *Chemical Engineering Science* 43, 1677–1684.

Rao, A. B. and Rubin, E. S., 2002. A Technical, Economic, And Environmental Assessment Of Amine-based CO2 Capture Technology For Power Plant Greenhouse Gas Control. *Environ. Sci. Technol* 36, 4467–4475.

Ratcliff, G. A. and Holdcroft, J. G., 1963. Diffusivities of gases in aqueous electrolyte solutions. *Transactions of the Institution of Chemical Engineers* 41, 315–319.

Rochelle, G. T., 2009. Amine Scrubbing for CO2 Capture. *Science* 325, 1652–1654.

Rzehak, R. and Krepper, E., 2013. Closure models for turbulent bubbly flows: a CFD study. *Nuclear Engineering and Design* 265, 701–711.

Rzehak, R. and Krepper, E., 2015. Bubbly flows with fixed polydispersity: validation of a baseline closure model. *Nuclear Engineering and Design* 287, 108–118.

Rzehak, R. and Kriebitzsch, S., 2015. Multiphase CFD-simulation of bubbly pipe flow: A code comparison. *International Journal of Multiphase Flow* 68, 135–152.

Rzehak, R., 2016, Modeling of Mass-transfer in Bubbly Flows Encompassing Different Mechanisms. *Chemical Engineering Science* 151, 139–143.

Rzehak, R. and Krepper, E., 2016. Euler-Euler Simulation of Mass-transfer in Bubbly Flows. *Chemical Engineering Science* 155, 459–468.

Schumpe, A., 1993. The estimation of gas solubilities in salt solutions. *Chemical Engineering Science* 48, 153–158.

Sugai-Guérios, M. H., Mariano, A. B., Vargas, J. V. C., de Lima Luz, L. F. and Mitchell, D. A., 2014. Mathematical Model Of The CO_2 Solubilisation Reaction Rates Developed For The Study Of Photobioreactors. *Canadian Journal of Chemical Engineering* 92, 787–795.

Stumm, W. and Morgan, J. J., 1996. Aquatic Chemistry: Chemical Equilibria and Rates in Natural Waters. *Wiley*, 3rd ed.

Tsonopoulos, C., Coulson, D. M. and Inman, L. B., 1976. Ionization Constants of Water Pollutants. *Journal of Chemical & Engineering Data* 21, 190–193.

Vaidya, P. D. and Kenig, E. Y., 2007. CO2-Alkanolamine Reaction Kinetics: A Review of Recent Studies. *Chemical Engineering & Technology* 30, 1467–1474.

Van Krevelen, D. W. and Hoftijzer, P. J., 1948. Kinetics Of Gas-Liquid Reactions Part I. General Theory. *Recueil des travaux chimiques des Pays-Bas* 67, 563–586.

Versteeg, G. F. and van Swaaij, W. P. M. 1988. Solubility and diffusivity of acid gases (CO2 and N2O) in aqueous alkanolamine solutions. *Journal of Chemical & Engineering Data* 33, 29–34.

Versteeg, G. F., van Dijck, L. A. J., and van Swaaij, W. P. M., 1996. On the Kinetics Between CO2 and Alkanolamines both in Aqueous and Non-aqueous Solutions. An Overview. *Chem. Eng. Comm.* 144, 113–158.

Wang, X., Conway, W., Burns, R., McCann, N., Maeder, M., 2010. Comprehensive Study of the Hydration and Dehydration Reactions of Carbon Dioxide in Aqueous Solution. *J. Phys. Chem. A* 114, 1734–1740.

Weisenberger, S. and Schumpe, A., 1996. Estimation of Gas Solubilities in Salt Solutions at Temperatures from 273 K to 363 K. *AIChE Journal* 42, 298–300.

Westerterp, K. R., Swaaij, W. P. M. V. and Beenackers, A. A. C. M., 1987. Chemical Reactor Design and Operation. *Wiley*.

Zeebe, R. E. and Wolf-Gladrow, D., 2001. CO_2 in Seawater: Equilibrium, Kinetics, Isotopes. *Elsevier Science*.

Zeebe, R. E., 2011. On the molecular diffusion coefficients of dissolved CO_2, HCO_3^- and CO_3^{2-} and their dependence on isotopic mass. *Geochimica et Cosmochimica Acta* 75, 2483–2498.

Zhang, D.-S., Deen, N. G. and Kuipers, J. A. M., 2009. Euler-Euler Modeling of Flow, Mass Transfer, and Chemical Reaction in a Bubble Column. *Industrial & Engineering Chemistry Research* 48, 47–57.